TAMPEREEN TEKNILLINEN YLIOPISTO
TAMPERE UNIVERSITY OF TECHNOLOGY
Julkaisu 482 • Publication 482

Erkki Levänen

Alumina Membranes – Colloidal Processing and Evolution of Functional Properties

Tampere 2004

Tampereen teknillinen yliopisto. Julkaisu 482
Tampere University of Technology. Publication 482

Erkki Levänen

Alumina Membranes – Colloidal Processing and Evolution of Functional Properties

Thesis for the degree of Doctor of Technology to be presented with due permission for public examination and criticism in Konetalo Building, Auditorium K1702, at Tampere University of Technology, on the 18th of June 2004, at 12 noon.

Tampereen teknillinen yliopisto - Tampere University of Technology
Tampere 2004

ISBN 952-15-1197-4 (printed)
ISBN 952-15-1411-6 (PDF)
ISSN 1459-2045

PREFACE

This work was carried out in Institute of Materials Science at Tampere University of Technology mainly during the period 1994-2000 as a part of the "Synthesis and properties of high performance ceramic oxides with on porous structures: membranes, filters and bio ceramics" project, which was part of the national programme on "Materials and structure Research" funded by the Academy of Finland. The research however has several by-products in National Technology Agency (Tekes) and industrial projects.

I wish to express my deepest gratitude to Professor Tapio Mäntylä for his continuous encouragement and continuous support throughout the work. Very special thanks also go to Professor Jarl B. Rosenholm, of Åbo Akademi University, for the long and deep discussions related to the field of physical chemistry and colloidal processing.

I am deeply grateful to M.Sc Pasi Mikkola and Dr. Niina Laitinen for their very fruitful co-operation and interesting discussions in the field of physical chemistry and membrane filtration. Special thanks also go to Lic. Tech. Antti-Pekka Nikkilä for the fruitful discussions and numerous advice during this long project. My sincere thanks also go to all the co-workers in the Institute of Materials Science. Due to the very long period of research time very many persons have helped me during this work. It is impossible to thank all in person since during this project some have left the Institute, some have been and moved on to positions in Finland and others to several to foreign countries around the world. I would like to thank them all. The enjoyable working atmosphere is due to them all. I would also like to thank all my friends for their support and encouragement. Special thanks go to biker friends of FFMC.

Financial support provided by Science foundation of City of Tampere (Tampereen kaupungin tiederahasto) is acknowledged.

Finally I would like to thank Pirjo for her listening skills and incredible patience during this long project.

Erkki Levänen Tampere, January 2004

Alumina Membranes – Colloidal Processing and Evolution of Functional Properties

ABSTRACT

In this thesis the whole preparation cycle of the ceramic alumina membrane is studied. The study is focused on colloidal processing with different additives, modelling of absorption on multiplayer substrate and on layer growth during dip coating and the effect of colloidal processing on growth kinetics. Other focus is laid on sintering and its effect on functional properties such as pore size, pore morphology and permeability. The prepared membrane performance is studied in different industrial processes.

Studies were done with submicron alumina powders having different purity grades. The deflocculation behaviour was studied with electrostatic and electrosteric mechanisms by using pH control and a polyelectrolyte as dispersant. The verification of the absorption model led to finding that the wetting behaviour of the solution deviates from the prediction of the Young equation. The effect of reduced capillary pressure with polyvinyl alcohol (PVA) addition can be clearly seen from layer growth rates. The used polyelectrolyte, sodium polymetacrylic acid (Na-PMAA) did not fully deflocculated the dip coating slip and resulted in fast and hard-to-control layer growth and highly porous membrane layer.

Sintering studies showed that at high sintering temperatures, where shrinkage should occur, the pore size coarsens and the size distribution broadens for supported particulate film, while the macroscopic densification is almost insignificant. Small deviations from ideal packing are suggested to lead to local densification, which causes pore size growth and broadening of distribution. Local densification also leads to pore channel straightening, which was found in the analysis of permeability values.

The alumina membranes were tested with several applications. The filtration tests were conducted for different industrial wastewaters. Feeds varied from paper mill wastewaters, stone cutting wastewaters, oily waters to dwell waters.

TABLE OF CONTENTS

LIST OF PUBLICATIONS

The thesis is based on the experimental work presented in detail in the following 6 papers: In the text these publications are referred with the corresponding Roman numerals.

I P. Mikkola, P. Ylhä, E. Levänen and J. B. Rosenholm, Effect of Impurities on Dispersion Properties of alpha-alumina Powder. Ceramics International 30 (2004) 291-299.

II E. Levänen, T. Mäntylä, P. Mikkola, and J. B. Rosenholm, Influence of Additives on Capillary Absorption of Aqueous Solutions into Symmetric Porous Ceramic Substrate. Journal of Colloid and Interface Science 234 (2001) 28-34.

III E. Levänen, T. Mäntylä, P. Mikkola and J. B. Rosenholm, Layer Build-up onto Two-layered Porous Substrate by Dip-Coating: Modelling and Effect of Additives on Growth Rate. Journal of Colloid and Interface Science 230 (2000) 186-194.

IV P. Mikkola, E. Levänen, T. Mäntylä and J. B. Rosenholm, Colloidal Processing of Aluminum Oxide Powder for Membrane Applications, Ceramics International 29 (2003) 393-401.

V E. Levänen and T. Mäntylä, Effect of Sintering Temperature on Functional Properties and Microstructure of Free-standing and Supported Alumina Membranes, Journal of the European Ceramic Society 22 (2002) 613-623.

VI N. Laitinen, A. Luonsi, E. Levänen, L. Grönroos, T. Mäntylä and M. Nyström, Modified and unmodified alumina membranes in ultra filtration of board mill wastewater fractions, Desalination 115 (1998) 63-70.

Author's contribution

The author's contributions to the above mentioned publications were as follows. In Paper I: helping in the planning of tests and assisting with the interpretation of results. Paper II: main researcher and writer. Planning and conducting experiments, interpretation of results and preparation of manuscript. Paper III: main researcher and writer. Planning and conducting experiments, interpretation of results and preparation of manuscript. Paper IV: dip coating, interpreting of results and writing of manuscript. Paper V: Main researcher and writer. Paper VI: Preparation of membranes, analysis of fouling layers, assisting with the interpretation of results.

Publications on the research area but not included in thesis

E. Levänen, M. Kolari and T. Mäntylä, Preparation of Sprayed Alumina microfiltration Membranes, Third International Conference on Inorganic membranes, Worcester, Massachusetts, USA, July 10-14, 1994, 4 p.

E. Levänen, M. Kolari and T. Mäntylä, The Effect of Raw Material Powder to the Properties of Alumina Microfiltration Membrane, Eighth Cimtec, World Ceramic Congress, Florence, Italy, June 29 - July 4, 1994, 8 p.

L. Grönroos, M. Kolari, E. Levänen and T. Mäntylä, The Effect of Sintering Temperature on the Structure of Thin Porous Alumina Layers, in Fourth Euro-Ceramics (ed. C. Galassi), Italy, Vol. 2. 1995, pp. 127-132.

E. Levänen, T. Koiranen, A.-P. Nikkilä, L. Grönroos and T. Mäntylä, Static Corrosion of Alumina Membranes, The Second Nordic Seminar of Membranes, Materials and Processes, Oslo, Norway, April 18-19, 1996.

N. Laitinen, D. Michaud, C. Piquet, N. Teilleria, A. Luonsi, E. Levänen and M. Nyström, Effect of Filtration Conditions and Back flushing on Ceramic Membrane Ultra filtration of Board Industry Wastewaters, Separation and Purification Technology 24 (2001) 319-328.

N. Laitinen, A. Luonsi, E. Levänen and M. Nyström, Effect of Backflushing Conditions on Ultrafiltration of Board Industry Wastewaters with Ceramic Membranes, Separation and Purification Technology 25 (2001) 323-331.

A. Luonsi, N. Laitinen, K. Beyer, E. Levänen, Y. Poussade and M. Nyström, Separation of CTMP Mill-Activated Sludge with Ceramic membranes, Desalination 146 (2001) 399-404.

N. Laitinen, M. Kulovaara, E. Levänen, A. Luonsi, N. Teilleris and M. Nyström, Ultrafiltration of Stone Cutting Mine Wastewater with Ceramic Membranes – a Case Study, Desalination 149 (2002) 121-125.

LIST OF SYMBOLS AND ABBREVIATIONS

ε	Porosity
ε_{cs}	Porosity of coarse substrate
γ_{lv}	Liquid surface tension
γ_{sl}	Surface energy of solid-liquid interface
γ_{sv}	Surface energy of solid-vapour interface
η	Viscosity
τ	Tortuosity factor
φ_0	Volume fraction of solids in slip
φ_c	Volume fraction of solids in cake
φ_{c2}	Volume solid fraction in growing layer
ϕ	Volume fraction of solids in the porous structure
θ	Wetting angle
r_H	Hydraulic radius
k	Kozeny-Carman constant
k_0	Kozeny-Carman pore shape factor
k_t	Kozeny-Carman pore tortuosity factor
G_T	Total free energy
G_b	Grain boundary free energy
G_s	Surface free energy
G_V	Grain volume free energy
L	Membrane layer thickness
L_c	Cake thickness
L_{c1}	Thickness of the layer formed during intermediate layer filling
L_e	Pore path length
L_{il}	Thickness of the intermediate layer
L_{tl}	Thickness of top layer
L_p	Penetration depth
L_{pcs}	Penetration depth of filtrate into the coarse substrate structure
K	Permeability
K_c	Permeability of the cake
K_{c1}	Permeability of the layer formed after intermediate layer filling
K_{c2}	Membrane layer permeability
K_{cs}	Permeability of the coarse substrate
K_{il}	Permeability of the intermediate layer
K_{tl}	Permeability of the top layer
K_1	Permeability of the substrate
P	Pressure
P_c	Capillary pressure
ΔP_{c1}	Pressure drop of the layer formed after intermediate layer filling
ΔP_{c2}	Pressure drop of the membrane layer
$\Delta P_{cap,cs}$	Capillary pressure created by the coarse substrate structure
ΔP_{cs}	Pressure drop of the coarse substrate
ΔP_{il}	Pressure drop of the intermediate layer
R_p	Pore radius

S_v	Surface area of volume unit
t	Time
BET	Surface area analysis method (Brunauer, Emmet, Teller)
CRP	Constant drying rate period
DLVO	Theory of the interparticle forces (Derjaguin, Landau, Verwey, Overbeek)
FRP1	First falling rate period
FRP2	Second falling rate period
i.e.p.	isoelectric point
SEM	scanning electron microscopy
TEM	transmission electron microscopy
XRD	X-ray diffraction
XRF	X-ray fluorescence analysis

1 INTRODUCTION

The demand for zero effluent industry has raised the importance of the reuse of solvents and non-reacted raw materials. In the chemical, pulp and paper and power industry there are several programs running that target the reduction of effluents and closing of the processes. The membrane technology offers a concentration method without phase transformation and hence needs only a low amount of energy. A membrane is defined as a semi permeable, perm selective film, which can be used in liquid applications for removing colloidal particles, organic molecules or dissolved salts. Applications with a gaseous phase membrane can be used for the removal of particles from gas streams or even separation of gases. Combined with catalytic materials the membranes are also used in membrane reactors as catalytic carriers or as perm selective catalytically active barriers [1-6].

To achieve optimum operation efficiency of membranes each application sets specific requirements for membrane structure and properties. The key factor is to understand the relation between membrane properties and structure. This requires strict control over the different stages of the membrane manufacture. The processing parameters have a strong effect on the properties and structure of the final membrane. The functionality of the membrane is governed by size, morphology and tortuosity of the pore channels, whereas physical properties such as strength and hardness with chemical properties define the long-term stability of the membrane. The long-term stability against degradation and fouling depends primarily on the chemical nature of the selected material, but also very strongly on the architecture of the membrane structure. Understanding the relation between processing and properties offers the tool for tailoring the membrane for each application with high performance.

A large variety of materials can be used for the preparation of membranes. The use of polymeric membranes is limited only to mild environments and low temperatures. However polymeric membranes are the most frequently used and there is large selection of membranes commercially available. Due to the high cost of inorganic membranes the use is concentrated on applications were polymeric membranes do not survive. The inorganic group, metals, carbon, carbides, nitrides and oxides can be utilized. Oxide membranes are frequently used because of their good thermal and

chemical stability. The hydrophilic nature of oxides makes them an obvious selection in aqueous applications.

General requirements for the membranes are high permeability, good separation i.e. sharp cut-off value, and long lifetime. The ceramic membranes fulfil these requirements well. The permeability is high due to multi-layered, asymmetric architecture of membrane structure combined with high porosity. The thin filtration layer with narrow pore size distribution leads to the sharp cut-off value. The strength of the ceramic materials enables the use of high trans-membrane pressures and cleaning by back-pulsing due to incompressible structure. The high strength results also in high hardness, which increases the erosion resistance and therefore the lifetime of the membrane. The more or less covalent bonding of the atoms also makes the ceramic materials chemically stable. The chemical stability makes possible the utilization of chemically aggressive cleaning methods. Furthermore the thermal stability enables the use of steam or high temperature to sterilize the membrane for biomedical or pharmaceutical use. Despite the advantages the ceramic membranes have severe disadvantages, which reduce the suitability of ceramic material for certain applications. The fragile nature of ceramics must be considered in designing and manufacturing of the membrane elements and modules.

This thesis concentrates on the relations between preparation and properties of the aluminium oxide membrane. The current situation of the membrane preparation and the general requirements for membranes are presented in the literature survey section. The literature survey is focused on the preparation method based on the packing of particles from dispersions on a rigid substrate followed by partial sintering. Each preparation step, raw material selection, colloidal processing, coating, drying and heat treatment, has several phenomena and parameters covering the fields of inorganic, organic and physical chemistry, thermodynamics, materials science and several fields of engineering. The focus of this thesis is therefore limited to colloidal processing, membrane layer formation and sintering steps. The experimental part includes the results and discussion of the studies focused on the relations between preparation parameters and final properties. Special attention is laid on the effect of the colloidal processing and additive system on the membrane formation and properties. Other focus is on the sintering behaviour and evolution of functional properties.

2 CERAMIC MEMBRANES

The membrane can be described as a semi permeable barrier between two phases that prevent intimate contact. The barrier restricts selectively the movement of particles or molecules through membrane. The selectivity can be based on size exclusion, differences in diffusion coefficient, in electrical charge, in solubility or in adsorption. The driving force for separation is usually pressure gradient [7].

The solid-liquid separation method by filtration is typically based on the particle size and can be divided into screen or particle filtration, micro-filtration, ultra-filtration and reverse osmosis as shown in Figure 1. Low-pressure reverse osmosis is often called nano-filtration [3]. The classification is based on the pore size and size of species to separate [3]. Ceramic filter elements are manufactured for all categories except reverse osmosis.

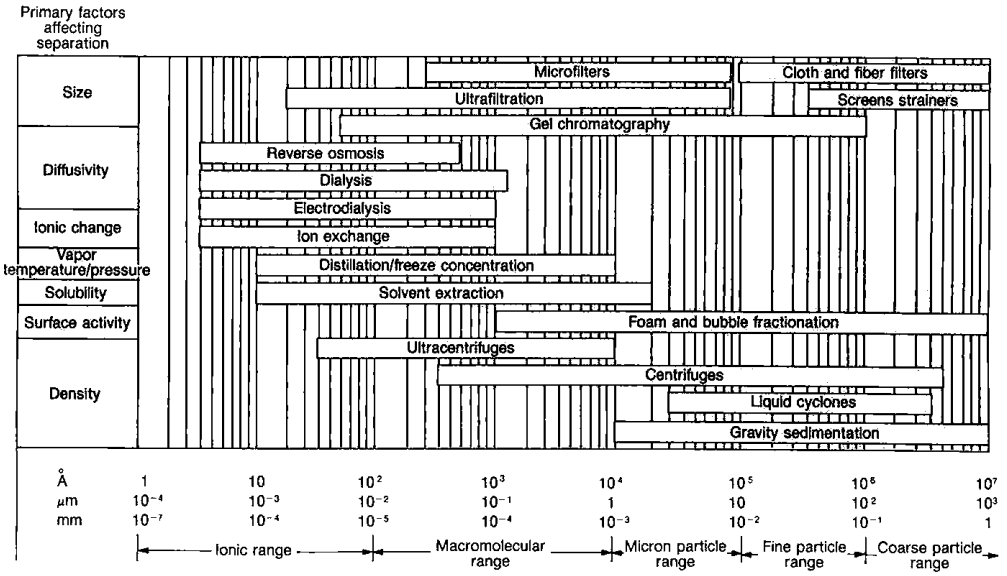

Figure 1. Classification of solid-liquid separation techniques [4].

2.1 Structure of the ceramic membranes

Membranes can also be categorized according to their structure into porous or dense membranes. The porous membranes are typically used for solid-liquid and solid-gas

separation, but gas separation applications also exist. The structure of a porous ceramic membrane can be symmetric when the pores are equally sized through the structure or asymmetric when pore size gradually decreases towards the surface where separation occurs. Pores can be straight through the structure having a constant diameter. The latter structure is typical for track etched membranes or membranes prepared by anodic oxidation. Usually the membrane structure is a 3-dimensional interconnected network of irregular pores. This kind of structure can be prepared by the packing of particles, by phase separation followed by leaching or by using polymeric sponge as slip casting mould [7].

Dense membranes are used for gas separation, the typical permeate is either hydrogen or oxygen. The most frequently used dense membranes are Pd based supported thin metal films, having good H_2 permselectivity. Almost dense SiO_2 membranes are used in membrane reactors such as H_2 selective barriers [8]. The oxygen transportation in zirconium oxide at high temperature is one example of ceramic dense membranes [9]. Also the structures where the liquid transport medium is immobilized into a porous matrix are included with dense membranes [1].

The structure of a membrane can be further modified to obtain enhanced permeability or separation factor. Modification of the surface can be applied to internal pore surfaces or on the top of membrane to prevent adsorption of impurities causing fouling or to improve the surface diffusion of adsorbed gases at gas separation membranes [10,11]. The modification can also reduce the pore diameter to the desired size or it can have catalytic properties [8].

The ceramic membranes can be manufactured to different configurations used as filtering elements. The most common type is the tubular element where the membrane surface usually exists on the inner surface of the tube. A membrane surface can also be prepared on the outer surface as in the case of hot gas filters. Tubular flow channels can be prepared as multi-channel monolith elements where substrate monolith has several membrane coated flow channels as demonstrated in Figure 2. Tubular configuration allows easy arrangement for the use of cross-flow conditions during filtration, but the packing density e.g., surface area-volume ratio, remains low. Dense packing of flat sheet membranes leads to high surface area to volume ratio but

the problems are arise from the cross-flow conditions and sealing of the stacks [3,5-7].

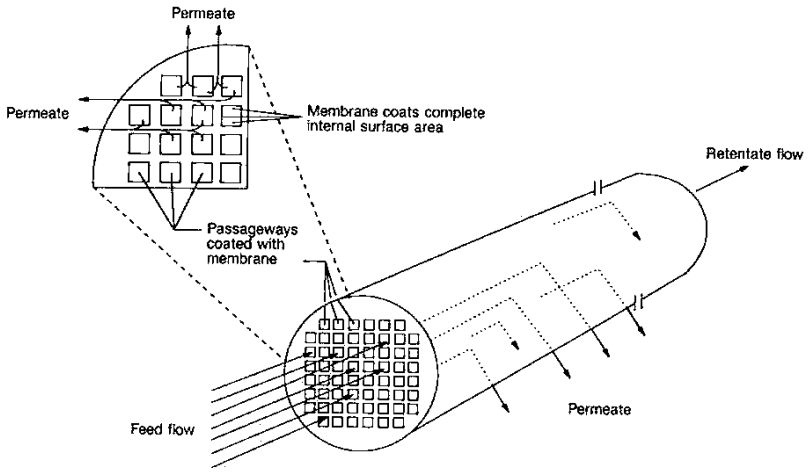

Figure 2. Schematic presentation of a multi-channel monolith membrane element [4].

2.2 Manufacturing methods of the ceramic membranes

Several methods for ceramic membrane preparation are developed each resulting in different pore properties [2,6,12-14]. The ceramic membranes with straight pores can be prepared with the track etching method and anodic oxidation. Membranes having an interconnected pore network can be prepared by phase separation and leaching, pyrolysis or by sintering of particles.

The track etching method is used mainly in the production of polymeric membranes, but some ceramic membranes have been made by this method. Thin films are bombarded with highly energetic particles from a radioactive source. Particles leave tracks, which are sensitive for etching and can therefore be leached away. The pore size can be varied from less than one nanometre to few micrometers. The track etching method has been used for example for mica and silicon nitride [6].

Anodic oxidation is used to prepare thin unsupported alumina membranes with symmetric or asymmetric structure. Aluminium foil is anodically oxidized in an acid electrolyte. The pore size can be varied by voltage used and by the type of acid. After anodic oxidation the remaining aluminium foil is leached away and the obtained porous alumina foil is treated in hot water to increase chemical resistance. The membranes manufactured by anodic oxidation are mainly used only in laboratory scale, since manufacturing of large areas with support is difficult [12].

In phase separation and leaching method is used a glass mixture with miscibility gab in phase diagram. At first the glass mixture melted to achieve homogenous melt. During cooling the phase separation results two in phases having an interconnected three-dimensional structure. The more soluble phase is leached away and the chemically more resistant phase is left to form a porous structure. The pore size obtained from the phase separation and leaching method can be varied from a few nanometres up to 200 nm. This method can be used for the preparation of complex shapes by glass forming methods [6, 13].

In the pyrolysis of silicon rubber a partly cross-linked structure of Si-O chains is formed. The structure is further oxidized in air at an elevated temperature to form SiO_2 [14]. The silica structure has a pore diameter of 5 to 10 nm and porosity around 50 %. A disadvantage of this manufacturing method is the high shrinkage during pyrolysis that easily results in the cracking of the structure.

2.2.1 Ceramic membrane preparation by partial sintering of particles

Particle packing followed by partial sintering is the most frequently used method for ceramic membrane preparation. Method is used for preparation of asymmetric, multi-layered membranes having tortuous capillaries. Preparation can be divided into preparation of the substrate structure and coating of the intermediate and the top layers. The substrate preparation is usually done by the classical shape forming methods of ceramics. The intermediate layer(s) and top-layer are usually prepared by dip-coating methods using conventional powders or sol-gel method [6,7,15]. The schematic presentation of a tubular, asymmetric membrane is shown in Figure 3.

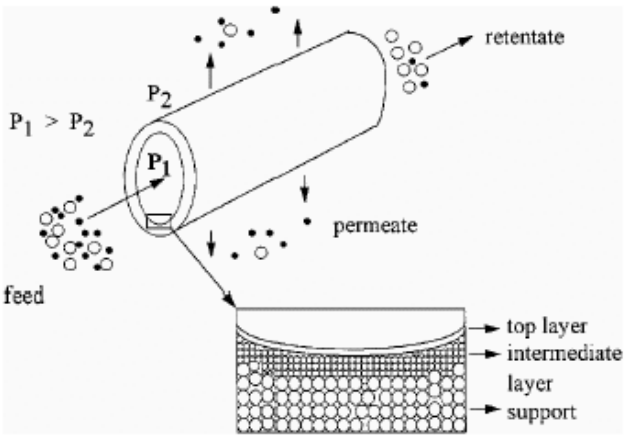

Figure 3. Schematic presentation of tubular asymmetric membrane [16]

The selection of raw material powder is of high importance in determining the properties of the resulting structure. The final pore size of substrate is from 0.1 to 0.6 times smaller than the particle size of the raw material powder. The powder morphology has an effect on that ratio since the packing of the spherical particles is more uniform compared to the packing of randomly shaped particles.

The substrate structure usually has a large pore size from hundreds of micrometers down to few micrometers depending on the application. Thickness is typically 1-5 mm. The requirements for the substrate are adequate strength, high permeability, corrosion resistance, narrow pore size distribution and good surface quality without defects. The substrate gives the strength for membrane structure, that should remain without remarkable deterioration during the life-time of membrane. Good surface quality and narrow pore size distribution of the substrate is needed to achieve defect free intermediate or top layers. Combination of these requirements is usually a design and optimisation task [17].

Main shaping methods for the substrates are extrusion and tape-casting [18,19]. Pressing and slip casting are also used [17]. Extrusion is used for the preparation of tubes or multi-channel honeycomb structures and tape-casting is suitable for flat

structures. After shaping the green body is consolidated by sintering. Both the extrusion and tape-casting methods need large amounts of organic additives such as binders, plasticizers, lubricants, antifoaming agents etc. for the preparation homogenous mass with suitable flow properties for the shaping process and further to ensure the handling of the green compact before sintering. These additives are removed during the early stage of sintering before the actual densification. Sintering is done typically at high temperatures to allow sintering of further layers at lower temperatures. When the substrate is made from rather fine particles, size < 10 μm, the structure can usually be consolidated by sintering without additives. When larger grains are used the inorganic binder, typically glass, is needed to achieve adequate strength via liquid phase sintering. Reaction bonding may also be used to replace the chemically weaker glass binder. In this method fine aluminium powder is oxidized during sintering, this acts as an inorganic binder [16].

Intermediate layer or layers are used to decrease the pore size of support in order to prevent penetration of very fine particles used on top-layer preparation. Requirements for the intermediate layer are smooth surface, narrow pore size distribution and surface homogeneity. To obtain homogenous formation of the top layer the intermediate layer should also have homogenous wetting behaviour and permeability [16,17]. The ratio between substrate pore size and intermediate layer pore size is typically from 10 to 30. The intermediate layer thickness should be as thin as possible but usually 100-1000 times the pore diameter is needed to obtain homogenous structure without defects [20].

The intermediate layer and top-layer are formed usually by dip-coating. The formation of layer occurs by capillary colloidal filtration in which the liquid phase of slip penetrates into the substrate by capillary suction while the particles of the slip accumulate on the surface of the substrate and form a continuous layer or cake. The cake formation is controlled by the solid content of the slip, viscosity of the liquid phase of the slip, the degree of deflocculation and the additive system of the slip. After drying the layered structure is sintered to achieve final properties. The effect of these parameters on layer properties is presented in more detail in the next chapter.

The top layer of the membrane structure can be prepared from fine powders similar to the intermediate layer or by the sol-gel method. In the sol-gel method colloidal or polymeric routes are used. The colloidal route is based on the synthesis of colloidal particles by condensation reaction from metal salts or metal-alkoxides. The colloids are packed on the substrate by dip coating, the solid content of the sol increases and causes the gelling. The gel layer is dried and calcined to achieve the inorganic structure [6,15].

With polymeric sol the polymerization reaction, usually hydrolysis followed by condensation, continues resulting in branched clusters growing from precursors at organic solvent. As polymerisation proceeds, the clusters finally form a three-dimensional network at the gel stage. During solvent removal the gel structure starts to collapse due to stresses caused by capillary pressure. After certain deformation and polymerization the mechanical strength has increased to the level which withstands stresses rising from surface tension. After drying the structure is calcined and sintered to obtain the final membrane structure. The polymeric route leads usually to amorphous, microporous structures. Heat treatment at high temperatures crystallizes the structures, but due to grain growth the pore size may increase into the mesoporous range.

In sol-gel technology the use of template agents has been introduced recently [15]. Organic groups or molecules are incorporated into the gels during sol-gel transition. Organic additives generate a residual porosity to the final structure after they are leached or burned out under heat treatment. The pore volume, pore size and pore morphology can be affected by the selection of templates such as surfactants, large organic molecules, latex emulsions or hollow micro spheres [15, 21].

Recent development has moved towards gas separation ceramic membranes based on microporous silica, clay-like structures and zeolites. Typical applications are the membrane reactors in the chemical industry. Sol-gel derived microporous silica is based on very fine, around 0.5 nm, pores in almost dense silica film. Clay-like structures use the lamellar structure of clays for separation purposes. Zeolites have very well defined crystal structures with single sized intra crystal pore channels. The dimensions of these channels can be varied by processing techniques [8,16, 22].

2.2.2 Modifications of preparation method based on particle sintering

Substrate and intermediate layer can also be prepared from the same fine-sized powder by using pore forming templates [23]. In this method starch was added into tape casting slip in order to form large pores after burn out and sintering. The pore forming template increases permeability but may also decrease surface quality, which makes the preparation of further layers more difficult. Problems rising from a rough substrate surface can be avoided by preparing the intermediate layer separately by tape casting. Intermediate layer tape can be laminated onto the substrate and sintered together.

The asymmetric membrane structure based on several, distinct layers is the basic concept ensuring high permeability with a good separation factor. The asymmetric structure preparation has also been studied by single manufacturing step [24, 25]. In this method a slip with a broad particle size distribution is allowed to sedimentate. Large particles sedimentate fast and form bottom layer. A finer fraction sedimentates slower and forms a top layer with small pores. The resulting structure has a continuous pore size gradient from the bottom towards the top surface. The pore size gradient is however in the rather narrow range, of 20 to 300 nm. Also the sintering of pore size gradient structure may cause some warpage [24, 25].

The asymmetric multi-layered membrane structure is based on clearly separate layers with rather sharp interfaces in order to maximize permeability. In membrane reactor applications the selectivity can be partly controlled by the operating pressure. The reactions in membranes with catalyst usually require longer flow time to achieve proper conversion. This has led to structure where the membrane separation layer has been impregnated into the intermediate layer or layers as shown in Figure 4.

The structure presented in Figure 4 b ensures the long contact time of reactant with catalyst. The lower permeability and selectivity is compensated by more precise control of the reaction zone by the feed pressure of reactant. The infiltration of micro porous silica, zeolites etc., can be done by sol-gel or vapour deposition methods [8].

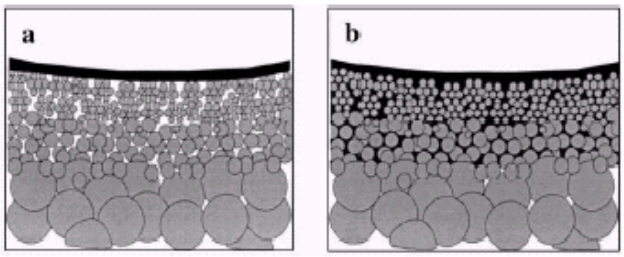

Figure 4. Schematic presentation of a) a thin supported separation layer and b) a infiltrated membrane in an asymmetric layer [8].

Another important recent innovation is the so called “chemical valve membrane” [8]. The membrane pore is infiltrated with a material which reacts with the environment and causes pore blocking or pore channel opening. One concept is to use the reversible red/ox behaviour of V_2O_5/V_2O_3 and related textural variations to regulate the membrane permeance [8, 26]

2.3 Key properties of the membranes

The functional properties of membranes mainly concentrate on the separation factor or retention and permeability of the film. These factors depend on the structure of the membrane and the morphology and characteristics of the pore network. The physico-chemical nature of the surface of membrane and pores also has a strong effect on the separation mechanisms and tendency for fouling i.e., permanent flux decrease. The mechanical properties and chemical resistance have great importance when using membranes for long periods in aggressive environments.

2.3.1 Pore size

The pore size is the distance between the two opposite walls of the pore. The size is not precise due to the highly irregular shape of pores. The pore size of the membrane is usually the narrowest opening through the structure or the pore entrance. The pore

size depends on the characterization method and pore size is therefore based on idealized pore models [6,27,28]. The pore structure is usually idealized to several simple configurations. Pores can be cylindrical, slit-shaped between packed slits or voids between packed spheres. Pore capillaries can be straight or tortuous and the pore radius can be constant or pore radius can change along the length. The porous structure can consist of pores going through the structure or blind pores, dead end pores having only one opening or closed pores that are not connected to other pores.

The pore size of a membrane is not uniform, since it has a size distribution. The narrow pore size distribution is favourable leading to the sharp retention properties. The distribution can be described by volume distribution, surface area distribution, number distribution or flow distribution.

2.3.2 Permeability

The fluid flow through the membrane structure defines in principle the economical efficiency of the membrane. The pure liquid permeability of membrane depends on the pore size, porosity, pore shape, pore tortuosity and thickness of porous structure.

The flow of incompressible fluid through the porous structure can be described with models such as d'Arcy law and as Poiseuille equation. The disadvantage of Poiseuille equation is that it assumes equally sized straight cylindrical pores. Permeability, K, can be expressed by Kozeny-Carman equation [29], which is based on the idea of hydraulic radius. Kozeny-Carman equation also takes into account the pore shape and pore channel tortuosity as follows:

$$K = \frac{\varepsilon r_H^2}{k} = \frac{\varepsilon^3}{k\ S_v^2\ (1-\varepsilon)^2} \tag{1}$$

where ε is porosity, r_H is the hydraulic radius and S_v is the surface area of the volume unit. Factor k is the Kozeny-Carman constant consisting of shape factor, k_0, and tortuosity factor, k_t. The pore shape factor values of 1, 1.4, 2 and 3 are commonly used for slit shaped pores, voids between randomly packed spheres, cylindrical pores

and spherical pores, respectively. The tortuosity factor, also marked as τ, describes the relation between actual pore path length, L_e, to shortest distance, L, measured along the direction of flow:

$$\tau = \left(\frac{L_e}{L} \right)^2 \tag{2}$$

For straight capillaries tortuosity is equal to unity, for other structures such as the bed of packed particles tortuosity is usually higher. For membranes packed from plate-shaped particles very high tortuosity factors have been reported [30].

The high permeability of the membrane is usually achieved by using asymmetric architecture presented earlier. The major part of flow resistance is formed in the separation layer having the smallest pore size. Therefore the separation layer is usually made as thin as possible. However in order to avoid straight through defects in the filtration layer, the layer has to be manufactured thicker at the cost of permeability.

2.3.3 Rejection

The rejection or retention is usually measured with model molecules like dextrans, proteins or polyglycols [6,28,30]. Filtration tests give the rejection of different molecular weight molecules. The cut-off value is defined as the molecular weight at which the 90 % rejection is obtained. Rejection measurements give a good description of the retention of molecules used in tests, but due to the different shape of molecules, membrane surface interaction with molecules, fouling and pore blocking of the membrane, test parameters such as pressure, temperature, cross-flow velocity the information of model molecule retention can not be directly used for real filtration applications.

2.3.4 Mechanical properties

The ceramic membranes have typically much higher mechanical strength compared to organic membranes. Mechanical strength allows the use of high pressures over the membrane and during the back pulsing [6, 18]. Due to the brittle nature of ceramics the stress concentrations must be avoided by proper designing of ceramic filter elements.

The strength is usually determined by bending or burst pressure tests. Bending tests give the strength of the material and burst pressure the maximum pressure inside the filter element. The strength of porous ceramic material is strongly dependent on the manufacturing procedure and selection of materials. The strength of the support structure is usually 20 to 200 N/mm^2. The requirements for the mechanical resistance of the top-layer rise from the erosive wear of fluid going trough and over the surface. When ultrasonic cleaning is used the top-layer is exposed to high mechanical stress. The mechanical resistance of the top-layer is usually determined by a hardness test, but the hardness does not directly tell the mechanical resistance in use.

2.3.5 Chemical resistance

Ceramic materials are considered to be chemically stable at a wide range of pH values due to more or less covalent atomic bonds and due to compactness of the crystal structure. Ceramics have highly negative free energy and a large total energy of formation. Despite the good chemical stability of ceramic material the porous, high surface area ceramic membranes are showing deterioration at aggressive environments [6,7,31,32]. In membrane regeneration processes where corrosive chemicals are used as the washing medium or in environments were aggressive fluid is filtered the chemical attack occurs.

The chemical attack may have effect on the permeability, retention or mechanical properties. The permeability may increase or decrease depending on the corrosive reaction on the membrane pore channels. Dissolution of the material usually increases permeability by enlarging the pore channels. Fluid media or impurities can also react with the membrane forming solid compounds that block the pore channels resulting in

permanent decrease of flux. The retention usually follows the pore size changes. Corrosion may also have an effect on the mechanical properties such as hardness and strength while having a minor effect on the functional properties. In this case the attack is concentrating to binder or necks between particles. The binder is usually the weakest link considering the chemical resistance. Particle-particle necks are sites where the minor impurities of raw materials are concentrating making the grain boundaries less chemically resistant. Even without additives or impurities the grain boundary has a loose structure allowing the dissolution to occur. The particle necks or binder bridges are also the narrowest places in the structure and even a slight loss of material can have strong effect on the mechanical properties [33, 34].

3 PREPARATION OF ALUMINA MEMBRANES BY PARTIAL SINTERING OF PARTICLES

The preparation of a thin porous alumina layer on the substrate using the dip-coating method is described in this chapter. The chapter considers powder selection, colloidal processing, film preparation, and the drying and sintering of films.

3.1 Powder selection

Raw material powder selection is the key step in membrane processing since the particle size has the strongest effect on the resulting pore size. The particle size distribution affects more the pore size distribution and final porosity. Since controlled packing is the aim, the uniaxial or spherical particle shape is usually favoured [16, 17, 24, 35]. The impurities have an indirect effect on the structure since they have an effect on the colloidal processing and sintering behaviour.

3.1.1 Particle size, distribution and shape

The pore size of a membrane is usually 0.1 to 0.6 times the size of the raw material particles, but the range broadens in the case of multi-modal particle size distribution or in the presence of agglomerates. The porosity depends on the packing type. The relative packing density of mono-sized spheres can range up to 0.74 in case of face-centred cubic packing. For random packing the relative densities are from 0.6 to 0.64 [36]. The lower value corresponds to the case of random loose packing. Broad or multi-modal particle size distributions increase the packing density resulting in smaller pore size [36, 37], which is not favourable in the case of membrane preparation. Narrow particle size is advantageous when seeking a narrow pore size with sufficient porosity of the membrane. The packing behaviour also has an effect on the drying shrinkage and sintering behaviour. Loose packing leads to large shrinkage during drying, this easily causes cracking of the film and the broadening of pore size distribution. During sintering high initial porosity easily leads to uneven and large shrinkage and defect formation.

The particle shape usually differs from spherical, which makes the exact estimation of the resulting pore size and porosity more difficult. Plate-like or elongated particles are easily orientated during the coating process and usually result in low packing density [36]. The raw material powder must therefore be selected so that the particles are as spherical as possible.

3.1.2 Purity

The purity of the powder has an effect on the slip preparation, sintering behaviour and chemical resistance of the final membrane. Impurities concentrated on the surface of particles effect the deflocculation behaviour due to surface charge variation. Pure alumina has i.e.p. around pH 8 to 9 and impurities like silica can move the i.e.p. towards the lower pH values [38]. During sintering the impurities have an effect on the diffusion or they may form a liquid phase between particles. Dissolved impurities or additives such as TiO_2 and MgO create vacancies in the alumina lattice and therefore strongly enhances the mobility of ions [39-41]. This increases significantly the densification rate and may result in coarsening of the pore/particle structure. Impurities that are not dissolved into lattice may form melt during sintering or they may react with the alumina or other impurities and form additional crystalline compounds. Excess TiO_2 may react to aluminium titanate ($AlTiO_5$) and excess MgO may form spinel ($Al_2O_3 \cdot MgO$). These compounds may hinder densification and cause thermal mismatch and cracking during cooling. Silica can react similar to mullite ($3Al_2O_3 \cdot 2SiO_2$), but at lower sintering temperatures it forms a melt with alumina especially when alkaline or earth alkaline oxides, Na_2O, K_2O, CaO are present [42,43]. This melt increases the densification rate and may cause coarsening of structure. These silica based glasses result in strong bonds between particles but have usually very poor chemical resistance compared with alumina. Other impurities also have a tendency to concentrate at the particle-particle necks causing chemical weakening of particle contacts or grain boundaries.

Alpha-alumina particles are produced by several ways each resulting in typical impurities. The conventional method is to prepare the powder by Bayer process, which produces normal-soda and low soda aluminas. The typical soda content is 0.1

to 0.6 % for normal soda grade and below 0.1 % for low soda grade. Other impurities are SiO_2 and Fe_2O_3. The particles exhibit a hexagonal plate-like structure 1.5 to 10 μm in size. Particle size can be further reduced by grinding [44].

High purity alumina, > 99.9 wt-%, can be prepared by modified Bayer process to have additional steps such as precipitation and repeated washing of the alumina which reduces the amount of soda, silica and iron oxide. In the preparation of alumina having purity over 99.99 wt-% the decomposition of high purity aluminium salts, sulphates, chlorides and nitrates, or aluminium metal is used. In the sulphate process Bayer hydrate is digested into sulphuric acid and then reacted with anhydrous ammonia to produce pure re-crystallised ammonium aluminate. After calcination a 99.99 wt-% pure alumina is obtained [44]. High purity alumina can also be prepared by the sol-gel route. Via hydrolysis of aluminium alkoxide the aluminium hydroxide is obtained. This oxide can be calcined to alpha alumina. The sol-gel route is commonly used in the membrane preparation, but for production of large quantities of powder sol-gel is uneconomical.

3.2 Colloidal processing

Colloidal processing follows after the powder selection. The aim of colloidal processing is to make dispersion or slip, which can be used for controlled membrane layer preparation in order to achieve the required film thickness and desired pore properties. In colloidal processing the aim is usually to de-flocculate or control the flocculation stage of the particles. Several additives such as dispersion agents, binders, plasticizers antifoaming agents, pore templates etc, make the colloidal processing step difficult to handle. The colloidal processing step has great importance when aiming at a defect-free membrane with desired functional properties. Anyhow in the papers published on membrane preparation only slight attention has been given to the colloidal processing. The focus is on powder selection, additive systems and sintering instead of the effect of colloidal processing in membrane formation mechanisms.

3.2.1 DLVO theory

The powder is dispersed usually into water. An oxide particle acquires a surface charge by the dissociation or protonation of surface OH groups to O^- or OH^{2+} groups. This surface charge depends on the pH and the electrolyte concentration. At low pH values the charge is positive and at high pH values negative. The point where the charge is zero is called the isoelectric point, i.e.p. The pH value of i.e.p. for oxide is dependent on the hydroxide structure of the surface. The surface charge is compensated by the counter charge, which surrounds the particles as a diffuse cloud. The surface charge layer and counter charge layer form the so-called electrical double layer. The thickness of this double layer is dependent on the dielectric constant of the medium and ionic strength of electrolyte solution.

The stabilization of suspension based on the charge of particles is called electrostatic stabilization. The well-known DLVO theory describes the inter-particle forces and predicts the total interaction potential which is the sum from van der Waals interaction and the electrostatic repulsion [45, 46]. Five different types of interaction are shown in Figure 5. The decrease of the surface charge, pH near i.e.p. or increase of salt concentration enhances the coagulation as shown in Figure 5.

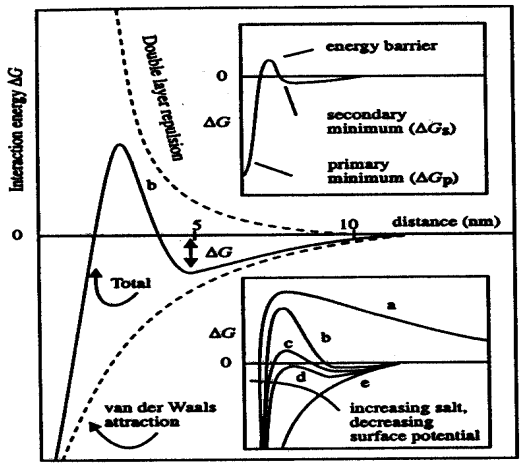

Figure 5. Interaction versus distance. (a) Stable dispersion, strong repulsion. (b) Secondary minimum exists, weak flocculation. (c) Stronger secondary minimum, small barrier to primary minimum, slow coagulation. (d) Very small barrier to primary minimum, secondary minimum exists, rapid coagulation. (e) Surfaces and colloids coalesce rapidly [20, 47].

The height of the energy barrier can be manipulated in an aqueous suspension of oxides by adjusting the pH, ionic strength, adsorption of complex ions and charged surfactants, poly-electrolytes etc. To achieve electrostatic stabilization without added dispersant, extreme pH values are often needed.

3.2.2 Additives

The interaction energy between particles in the dispersion can be manipulated by the adsorbing or non-adsorbing polymers. With adsorbing polymers there can be repulsion of the particles due to steric or electrosteric mechanisms, depending on the orientation and nature of the adsorbed molecules. Polyelectrolytes are probably the most commonly used for dispersing oxide powders in water. Polyelectrolyte dissociates in water and forms highly charged chains repelling each other. The degree of the dissociation is dependent on the pH of the water and electrolyte concentration. Dissociated chains adsorb on the surface of alumina due the electrostatic forces. The covered alumina particle show a highly negative charge at basic pH values indicating electrostatic stabilization. Sodium poly(metacrylic acid) (Na-PMAA) is a widely used polyelectrolyte for the stabilization of alumina suspensions [48-51]. Na-PMAA has many carboxcylic acid (COOH) sites, which dissociates in water and form negatively charged sites (COO^-). The degree of dissociation increases with pH and at pH 8.5 all functional groups are dissociated and the molecule has high negative charge [52, 53]. With the electrostatic stabilization mechanism the steric mechanism also exists. When two particles approach the polymer chains start to compress, which is observed as repulsion of particles.

Binders are added to the slip in order to prevent cracking during film drying and to give strength to the green film allowing easy handling. The binder forms organic inter-particle bridges after solvent evaporation. The binders have an effect on the several properties of the slip. They have an affect on the wetting behaviour, by changing the surface tension of the solution, increase viscosity of the solution and therefore reduce the sedimentation rate and layer build-up rate in slip casting or increase the film thickness in film coating processes. Requirements for binders are compatibility to the system, ability to function as a stabilization aid, ability to produce

a lubricant effect between particles, no interference between solvent evaporation, low glass transition temperature and easy burnout without leaving residues. For aqueous slips the most common binders are cellulose derivatives, polyvinyl binders and acrylics.

Polyvinyl alcohols (PVA, [-CH2-CH(OH)-]n) used as binders usually have a molecular weight of 13 000 to 100 000. PVA is non-ionic polymer, which has a typically low affinity on the oxide surface and has no effect on the isoelectric point of oxide. Commercial PVA is usually a mixture of polyvinyl alcohol and polyvinyl acetate (PVAc). The fully hydrolysed PVA, which have no acetate groups, is soluble only in the hot water. The presence of acetate groups enhances the solubility to water but also have an effect on the properties of PVA. The increase of acetate groups lowers the glass transition temperature and strength of the dried PVA and decreases the surface tension and viscosity of the solution. Polyvinyl alcohol normally requires a plasticizer such as glycerol or glycol to reduce the glass transition temperature [54-59].

3.3 Film preparation

The final composition of the slip must be optimised to the selected coating process, to the required film properties and take into consideration the properties of the substrate. The coating process should be able to produce a thin defect free layer having uniform thickness and controlled structure. The adhesion between substrate and membrane layer should be adequate. Several preparation techniques exist such as dip coating, tape casting, spin coating, spraying etc. The film formation mechanisms can be divided into two groups, capillary colloidal filtration and film coating [20]. In capillary colloidal filtration the dry, porous substrate is placed into contact with the slip that is wetting the substrate. The liquid phase of the slip is sucked into the pores of the substrate and the particles from the dispersion are accumulated on the surface forming a cake. This cake is dried and sintered to the final membrane. In the film coating process the layer is a result of the drag force exerted by the substrate during withdrawal from the dispersion. To obtain solely film coating mechanism the substrate should be dense or the capillary action of pores should be suppressed. The

principles of the capillary colloidal filtration and film coating processes are presented in Figure 6.

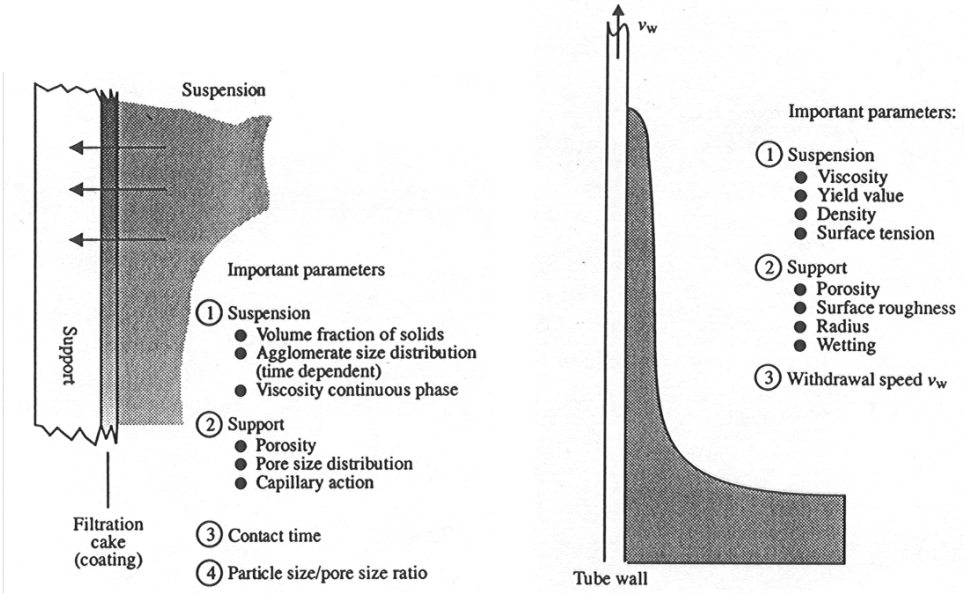

a) b)

Figure 6. Principles of a) capillary colloidal filtration coating and b) film coating processes [20].

3.3.1 Capillary colloidal filtration

The key parameters of the capillary colloidal filtration coating process can be divided into different groups. The slip parameters affecting the layer formation are the volume fraction of solids, particle or flock size and size distribution, viscosity of the liquid phase. These parameters have an effect on the cake growth kinetics by volume balance, permeability of the cake and by the viscous drag in the pores. The liquid phase properties affect the capillary pressure, which is the driving pressure of the system, by surface tension and wetting angle between pore walls of the substrate and the liquid phase. The substrate has an effect on the cake growth, porosity, pore size and wetting behaviour. Substrate porosity and pore size have an effect on the flow resistance that has a further effect on the cake growth dynamics especially at long coating times and low solid load slips. At long coating times the substrate flow resistance becomes important since the liquid phase of slip flowing into the substrate. Substrate pore size also affects the driving force of the cake growth since the capillary

pressure is created in the substrate. Capillary pressure depends on the pore size, liquid phase surface tension and the wetting behaviour between pore walls and liquid.

The layer growth kinetics have been intensively studied and modelled [60-66]. These models are usually developed for the modelling of the slip casting process. These models usually neglect the flow resistance of the substrate, but specific models have also been developed that consider the effect of the substrate. The thickness of the coated layer grows according to square root of time law [20]:

$$L_c^2 = \frac{2\Delta P t}{\eta\left(\frac{\varphi_c}{\varphi_0}-1\right)\left[\frac{1}{K_c}+\left(\frac{\varphi_c}{\varphi_0}-1\right)\Big/\varepsilon_1 K_1\right]} \tag{3}$$

Where L_c is cake thickness, ΔP is driving pressure, t is time, η is viscosity of liquid phase, φ_c is the volume fraction of solids in cake, φ_0 is the volume fraction of solids in slip, K_c is the permeability of the cake, K_1 is permeability of the substrate and ε_1 is the porosity of the substrate. The slip formulation has a strong effect on the layer growth rate as can be observed from Equation (3). If slip consists totally of deflocculated, separate particles, they tend to pack densely resulting on a high volume fraction of solids in the cake. The resulting pore size is also small leading to low permeability of the layer. In that case layer growth rate is slow. If the additive system simultaneously increases viscosity, decreases capillary pressure and allows particles to arrange in the layer during growth the resulting growth rate decreases drastically. These parameters allow preparation of a thin layer with uniform thickness so that the coating process is not very sensitive to contact time. The growth of the layer stops when the substrate is saturated and the driving pressure disappears or when the growth rate comes so small that the back-diffusion caused by Brownian motion overcomes the particle accumulation rate.

In preparation of multi-layered membranes the system is more complicated if the liquid penetrates to layers having different permeability and pore size. The driving force varies and the constant pressure drop caused by the different layers results in

deviation from the square root time growth law. The effect of multi-layered substrate on the layer growth has not been widely studied.

3.3.2 Film coating mechanism

In the film coating mechanism the major parameters are withdrawal speed of the substrate with the viscosity of the slip. The contact time is not relevant in film coating since capillary action is not present. Capillary action can be eliminated by filling pores with liquid or by hydrofobizing the pore surface. When the substrate, which the suspension is wetting, is drawn from the suspension the viscous drag forms a wet film layer. If the withdrawal speed is increased a thicker film is obtained. The increase of viscosity has a similar effect on the film thickness. The surface tension of the suspension has only a weak effect on the layer thickness. The layer obtained from film coating technique is wet film and the thickness of dry film is dependent on the solid load of suspension, the packing of particles during drying, flock size and additive system. Other parameters that have an effect on film coating are the properties of the substrate such as surface roughness and wetting [20]. During drying the solvent is evaporated and the re-arrangement of particles occurs. If the additive system is able to lubricate particle contacts, particles will rearrange to rather dense structure.

In dip coating based on capillary colloidal filtration the film coating mechanism is also present. The effect of the film coating mechanism on layer thickness is dependent on the viscosity and withdrawal speed as mentioned above.

3.4 Film drying

When the substrate is removed from the slip the drying begins. After coating based on capillary colloidal filtration the substrate is partly or totally impregnated by the liquid phase of the slip. The membrane layer consists of particles or flocks packed by the capillary action of the substrate and voids filled with solvent. The solvent starts to evaporate with the rate comparable to evaporating of pure liquid. The evaporation rate depends on the temperature, vapour pressure and vapour velocity along the surface.

The drying consists of several stages during which the particles may rearrange and defects may form [55, 67].

At constant drying rate period (CRP) the evaporation occurs from the rather flat outer surface. At the beginning the substrate feeds liquid to the wet layer causing shrinkage similar with capillary action produced by substrate pores. The additives of liquid may migrate and concentrate on the surface of the film. In this situation the permeability of the wet film layer may reduce the liquid flow to a solid vapour interface. When liquid meniscus retrieving from substrate reaches the wet film and substrate interface the shrinkage of the cast layer starts. At early stages the rearrangement of particles and the collapse of weak flocks occur. During evaporation of the solvent the solid content of wet layer increases resulting in increase in the viscosity of the film layer. Also the additive concentration increases leading to increase of viscosity of the liquid phase. The drying film reaches the viscoelastic point due to difficulties in particle movement. The liquid surface cannot any longer be flat on the scale of particles and a meniscus of liquid develops. The curvature of liquid menisci results in the compressive stress on the particle network causing shrinkage in order to minimize the liquid-vapour area. In supported film the compressive forces cause shrinkage only in direction normal to film surface if the friction or adherence between film and substrate is adequate. The one dimensional shrinkage results therefore in tensile stress into drying film.

At the end of constant drying rate period the shrinkage of film stops and the curvature of the menisci of liquid equals the pore radius. The evaporation rate decreases since evaporation occurs from curved interface inside the porous compact. This stage of drying is called the first falling rate period (FRP1). At FRP1 most of the evaporation occurs in the surface and liquid flows along capillaries to surface. When the liquid flow stops and the drying occurs via transport by vapour diffusion in the pores the stage of drying is called the second falling rate period (FRP2). The drying front is deep in the porous structure and drying rate is not very sensitive to external conditions. After drying the physically adsorbed solvent may remain in the surfaces of the pores. That will be removed in the early stages of sintering.

3.5 Sintering

Sintering of free-standing structures has been widely studied and modelled [17, 24, 68-74]. Need of information on the consolidation mechanisms in the case of restricted shrinkage has risen from several applications such as electronics, high temperature and wear resistant coatings, optical films, ceramic membranes etc. Both theoretical and practical approaches to the sintering of dense polycrystalline thin films have been done. The micro-structural characteristics of porous supported thin films are much less studied area [76-88]. The sintering of ceramic membranes is usually done at temperatures resulting in necks between particles. At these temperatures shrinkage is small and the structure does not significantly deviate from the structure in which shrinkage is not restricted. Some properties such as high hardness and good chemical resistance require thicker necks and therefore higher sintering temperature. The higher temperature leads to significant shrinkage and at these temperatures the differences between structures sintered on substrate and without restrictive substrate become significant.

3.5.1 Free-standing structure

The driving force for sintering is the reduction of total free energy, ΔG_T, of the system

$$\Delta G_T = \Delta G_V + \Delta G_b + \Delta G_S \tag{4}$$

Where ΔG_V, ΔG_b and ΔG_s represent the change in free energy associated with the volume, boundaries and surface of the grains, respectively. The major driving force in conventional sintering is ΔG_s and the ΔG_s has usually the greatest importance at the initial stage of sintering at which the membranes are usually sintered.

The consolidation by sintering can be divided into initial stage, intermediate stage and final stage depending on the micro-structural changes [75]. There is no clear distinction between the sintering stages. If the packing of particles deviates from the uniform packing and consists of wide particle size distribution, agglomerates, pores with large size distribution, chemical inhomogeneities etc. the sintering may proceed

at different stages at different regions. In the case of uniform packing the distinction between stages is not sharp.

At the initial stage of sintering shrinkage is very small. The strengthening of the structure occurs by the neck formation between particles. These necks form grain boundaries replacing the solid vapour interface. The initial stage of sintering continues until the ratio between neck diameter and particle diameter achieves the value of 0.3. The pore structure remains open and the pore shape becomes smoother and rounder [89]. Porosity does not significantly decrease. The kinetics of sintering is dominated by the curvatures near the inter-particle necks. The progress of initial sintering is usually monitored by the neck growth observations by microscopic methods or monitoring the decrease of surface area by gas adsorption method. The mass transport mechanisms related to initial stages of sintering are surface diffusion and evaporation-condensation. Neither of these mechanisms causes macroscopic shrinkage or densification. Particle spacing does not change due to mass flow originating and terminating at the particle surface. Surface diffusion dominates the sintering of many covalent solids. Evaporation-condensation occurs when sintering the materials having high vapour pressure.

In the intermediate stage, the significant shrinkage occurs leading to the decrease of porosity. The compact properties are developed in this stage. Pores shrink due to neck growth and particle centres approach and the pores become smoother still maintaining open network. The slow increase of grain size occurs and at the end of the intermediate stage the grain growth is rather rapid and might lead to pore isolation. The mass transport mechanisms related to intermediate stage of sintering are bulk transport mechanisms such as volume diffusion, grain boundary diffusion, plastic flow and viscous flow. At the solid stage sintering of crystalline materials such as alumina the grain boundary diffusion and volume diffusion are the major mass transport mechanisms. These mechanisms result in particle approach leading to shrinkage of compact.

Final stage of sintering is achieved when the three-dimensional pore network collapses to isolated spherical pores in grain boundaries. The porosity has shrunk to approximately 8 %. The densification rate decreases. The isolated pores shrink by

diffusion of trapped gas through solids. The shrinkage of large pores might be very slow. The grain size increases when the grain boundaries move. If the grain size movement is fast, the boundary may break away from the pores leaving spherical pores inside the grain.

Models for describing neck growth are based on the idealized neck shapes between two particles. The particle centre approach is usually derived from the neck growth and the amount of interpenetration of two particles. This two-particle model has been successful in categorizing the active material transport processes. However, problems arise when the two-particle model is attempted to extrapolate to real powder compacts. The model does not consider that in the real powder compacts the particles rearrange, contacts are forming and breaking up, pores are opening up during rearrangement processes. When the packing is close to uniform packing the deviation might be small. When the powder compact has variations in packing, asymmetric particle contact geometry and non-uniform particle size, pronounced rearrangement and stresses occur leading to significant deviation from shrinkage predicted by the two-particle model [72].

3.5.2 Restricted sintering

The use of multi-layered structures has focused the interest in the sintering of the constrained particulate film on a rigid support [76-82]. Bordia and Raj [76] have modelled the stresses that develop during the sintering of constrained particulate film. Their model is based on the assumption that the film is a linear viscoelastic solid with spherical isolated pores. They found that if the shear stress caused by densification and the resisting substrate, develops faster than the material can respond by relaxation, high tensile stresses may occur. These stresses are developed during the initial stages of sintering. The neck size is still small and stresses may lead to the formation of defects. The defect may be a brittle crack caused by the elastic strain energy or a crack grown by time dependent diffusional growth of pores. The crack formation can be avoided with large particle size and high sintering temperature. The large particle size anyhow reduces the densification rate. The small particle size favours the defect formation and the substrate reduces the densification rate. Garino and Bowen [77,78] studied the densification kinetics of the particulate film in the case

of viscous sintering, liquid phase sintering and solid state sintering. They assumed the material to be a viscous continuum. In the case of viscous sintering the model described well the densification of constrained film. The solid state sintering led to significantly lower density than predicted by the model. The grain growth alone did not explain the low density. Lower density was explained by the anisotropy during sintering resulting in the dense regions separated by the porous regions. Carroll and Rahaman [79] used the data of Garino and Bowen for testing a model, based on the cubic packing of spherical particles. Their model assumed that the material is transported from the top and the bottom necks to the side necks of the particles. They found that the densification rate of the constrained thin films is highly dependent on the dihedral angle of the material and on the grain growth. The grain growth can essentially stop the film from densification.

Micro-structural evolution in films of nanosized particles, especially titania, has been widely studied [83-87]. These studies have been focused on the densification, on the evolution of pore size and permeability, and on the effect of the substrate on the phase transformation temperature. These studies confirm that the substrate restricts the densification and the porosity decreases slower at higher temperatures compared with the free-standing films. The grain and pore size either increased or decreased probably depending on the particle coordination number. The local densification resulted in a strong grain growth. When the pore size increased the permeability usually increased, but the permeability data was not always available. The substrate typically increased the phase transformation temperature for the materials such as anatase-rutile transformation for titania. These papers however concentrated on the micro-structural evolution of the nano-particle sized supported films and the study of the functional properties was not deeply concerned.

Wang et al [88] have studied the effect of sintering temperature on pore size and permeability of alumina micro-filtration membranes. They also found the coarsening effect of membrane pores when sintered with substrate. The pore size coarsening was more pronounced in case of thin membranes. They also found that after sintering at high temperatures the permeability of membranes decreased significantly. They proposed that the permeability decrease was the result of pore number decrease with pore connectivity reduction although pore size increased continuously. They also

assumed the decrease of pore channel length. The porosity of the studied membrane films was not given. The permeability was studied on the basis of Poiseuille equation which includes pore size, pore length, pressure and viscosity but does not consider pore tortuosity or porosity.

4 AIM OF THE STUDY

In this thesis the objective is to prepare thin porous films on a porous substrate. This study has focused on defining the effect of process parameters on the properties of the alumina membranes for solid liquid separation. Several applications of particulate films, such as membranes, filters, coatings, catalytic carriers, thermal barriers, human implants etc., have different requirements for the structure of the material. The final structure can be controlled when we have knowledge of molecular interactions between solid surfaces, consolidation of powder dispersions and sintering behaviour of the films on rigid substrate. The knowledge of relations between processing and resulting structure allows tailoring of the membrane properties for different applications.

The processing steps are not separate and each step has an effect on the next processing step. This thesis concentrates on the colloidal processing, membrane layer formation by the capillary colloidal filtration method. The colloidal processing is the basis of membrane preparation and has significant effect on the layer formation. The layer formation is studied with slips having different colloidal processing parameters such as deflocculation stage, deflocculation mechanism, additive system, solid content etc. As the final stage the sintering cycle is studied. The effect of raw material powder and sintering parameters on final membrane properties are studied. The aim is to understand mechanisms affecting during restricted sintering e.g. sintering of thin film on rigid substrate. The main properties monitored in sintering studies are functional properties such as pore size, pore size distribution, permeability and hardness.

This study does not solve all the interconnections between processing, structure and properties, but aims finding tools and models to obtain desired membrane structures for solid liquid separation.

5 MATERIALS AND METHODS

As reviewed earlier several oxides can be utilized to prepare a ceramic membrane. In this study aluminium oxide was chosen as the model material. Other oxides have a similar type of behaviour and the results can be used as guidelines in the preparation of membranes with other oxide powders. The chosen particle size resulted in membranes with pore diameter of 70 to 500 nm, that falls into the region of ultra- and micro-filtration.

Alumina powder and additives used for membrane preparation are presented in this chapter. The membrane preparation methodology is also briefly presented as well as characterization techniques used in different stages of processing

5.1 Raw materials

Alpha alumina powders having different purity grades were used. The powder prepared by the Bayer process, Alcoa A16 SG (Alcoa Industrial Chemicals Europe, Bad Homburg, Germany), was the most impure having 99.57 % alumina with major impurities of Na_2O (0.082 %) and SiO_2 (0.122 %) measured by XRF. These impurities were traces from processing although the powder was low soda type. Baikalox CR 6 (Baikowski International Corporation, Charlotte, NC, USA) had higher purity 99.84 % having major impurities of Na_2O (0.022 %) and Cl (0.027 %). Silica was not found in this powder with XRF analysis. Some experiments were also done with high purity alumina, AKP-30 (Sumitomo Chemical Co., Ltd., Tokyo, Japan) having measured alumina content of 99.87 % according to XFR with major impurity of Na_2O (0.036 %) [I, III, IV, V]. The phase purity of as received powders were measured by XRD. The results showed that all powders were pure α-alumina. Transition aluminas, hydroxides or amorphous alumina were not found. In TEM-examination also only α-alumina was found [I].

The particle sizes of all powders were 0.3 to 0.55 μm according to manufacturer. The grounded Alcoa A16 SG had irregularly shaped particles and the broadest size distribution whereas AKP-30 had spherical particles and the narrowest size

distribution. The CR 6 powder consisted from hard agglomerates of spherically shaped primary particles. The mean agglomerate size distribution was 1 μm while the primary particle size was 300 nm [I, IV, V].

Deionised water was used as the solvent in all experiments. For deflocculation both electrostatic and electrosteric systems were utilized. For the electrostatic system nitric acid, HNO_3, was used. The electrosteric deflocculation was done mainly with sodium salt of poly-methacrylic acid, Na-PMAA from different manufacturers [I, III, IV, V]

Polyvinyl alcohol, PVA, (Fluka, Switzerland) with a molecular weight of about 22 000 g/mol was used as a binder to prevent the cracking of the membrane during drying. PVA was also used to alter the properties of the slip. In some experiments glycerol was used as a plasticizer [II, III, IV, and V]

Two substrate structures, symmetric and asymmetric, were used in dip-coating and absorption tests. Symmetric substrates had two different pore sizes: the coarse pore sized, d_{50} = 35 μm, silicate bonded alumina and the finer pore sized, d_{50} = 0.6 μm, alumina. Asymmetric substrates had the above mentioned finer alumina layer on the coarse pore sized substrates [II, III, IV, V]. For filtration experiments the filter element substrates were made from silicate bonded alumina by Outokumpu Mintec Oy, Turku, Finland [VI].

5.2 Membrane preparation methods

The membrane preparation can be divided into different stages: slip preparation, casting and sintering. These stages are briefly described below.

In slip preparation the dispersion agent was first dissolved to deionised water followed with the gradual addition of alumina powder under continuous mixing. This procedure was selected to obtain complete dispersion of powder. When the dispersion agent is first dissolved into the solvent the adsorption occurs fast on the added oxide powder. By using this method the risk of local flocculation of slip is minimized. When the required solid content was achieved the slip was milled for at least 12 hours in a planetary ball mill to ensure the complete deflocculation.

After deflocculation other additives such as binders and plasticizers were added. PVA binder was dissolved into the de-ionised water by boiling. Plasticizer was mixed into the binder solution and the binder-plasticizer solution was further mixed to the slip followed with gentle ball milling to ensure homogenous additive distribution.

The membrane layer preparation was done mainly by dip coating. In dip coating the substrate was placed into contact with the slip and the liquid phase of the slip started to penetrate into the substrate while the particles of the slip accumulated on the surface of the substrate. After a certain time the substrate was removed from the slip and the obtained membrane structure was ready for drying. The drying was performed overnight at room temperature to obtain slow drying needed to prevent cracking of the membrane film.

The sintering of membranes was performed in an electric furnace at ambient atmosphere. The temperatures were varied from 1000°C to 1400°C with different dwell times. The temperature rise rate was either 5 or 2 °C/min depending on the substrate structure. Some substrates were sensitive to heating rate and easily damaged if heating rate was too fast. Cooling was performed at the same rate as the heating. After the sintering cycle the membranes were ready for characterization.

5.3 Characterization methods

During the membrane preparation and in characterization of final membranes several parameters were monitored. The characterization methods described in this chapter concentrate on the methods used for evaluation of the membrane layer growth kinetics and characterization of the membrane properties.

5.3.1 Evaluation of membrane layer growth kinetics

The dip-coating dynamics were evaluated in two stages. Firstly we studied the penetration of pure polymeric solutions into the substrate structure [II]. The penetration rate was measured from the increase of sample weight during absorption. The penetration rate was further evaluated against the surface tension and viscosity of

polymeric solutions. From these relations the wetting behaviour between solution and the substrate pore walls could be calculated. The apparent capillary pressures were calculated from the solution absorption results. The calculated capillary pressures were used as the driving force during the membrane layer build up.

The membrane layer build-up kinetics was studied in a similar manner to the adsorption rate. The substrate was placed into contact on the slip and the increase of weight was monitored. After deposition the substrate with the dip-coated layer was dried and the weight increase measured. The thickness of the dip-coated layer was measured after drying. The porosity of dip-coated layer was calculated from the mass and the volume of the coated layer. The mass increase during dip-coating was converted to the layer thickness by using the measured porosity. As a result the dip-coated layer thickness versus the dipping time curve was obtained. The layer growth rate curves were further used for evaluation of membrane permeability during dip-coating [III, IV].

5.3.2 Membrane properties

Packing of particles and evolution of microstructure were monitored with density and porosity measurements. For density measurements Archimedes´ method was used for free-standing, sintered membranes [90-92]. The porosity and density of membrane layer are evaluated from the mass and volume of membrane layer by using the theoretical density of alumina.

Surface area of raw material powders and sintered, free-standing films were measured by N_2-adsorption. The powders were measured as received and the free-standing films were crushed to small pieces to allow the measurement. BET-method was used for surface area calculation from adsorption isotherm [93].

The pore size of membranes was characterized by two methods. Free-standing membranes were characterized by mercury porosimetry and supported membranes by flow pore test.

In Hg-porosimetry cleaned sample is immersed into mercury and the pressure of mercury is increased. Since mercury does not wet most of the materials external pressure is needed to force the mercury into the pores of the sample. During the increase of pressure the penetration volume of the mercury is measured and the intrusion curve is obtained. After intrusion the pressure is decreased and the extrusion curve is obtained. The intrusion curve is used in the calculation of pore size distribution according to Washburn equation [93]:

$$P = \frac{-2\gamma \cos\theta}{R_p} \tag{5}$$

where P = pressure of mercury

γ = surface tension of mercury

θ = contact angle between mercury and sample

R_p= pore radius into which the mercury penetrates

In measurements the 135° was used as contact angle and 485 mN/m as surface tension of mercury. The pore size obtained from the intrusion curve measures the pore openings between pore cavities. The size of the cavities behind the narrow opening is seen as pore volume of the measured opening. The pore size distribution hence describes the sieving properties of the membrane.

In the flow pore test the sample was wetted with liquid that wets the sample well. In this study ethanol was used as the liquid. The wetted sample was placed to manifold in which the pressure over sample and flow through sample could be measured. The pressure over the sample was stepwise increased and the flow was recorded. Compressed air was used as the measuring gas. With low pressures there was no flow through the membrane since the pressure was too low to expel the liquid from the pores. At the pressure determined by the Washburn equation the biggest pore opened and flow through the membrane started. When pressure was increased furthermore the smaller and smaller pores were opened for flow. In the end all the pores were dry. The dry flow through the sample was also measured. The drying of the samples was

ensured by heating in the oven. By comparing wet flow to dry flow the flow pore size distribution was obtained as presented at Figure 7 [94,95].

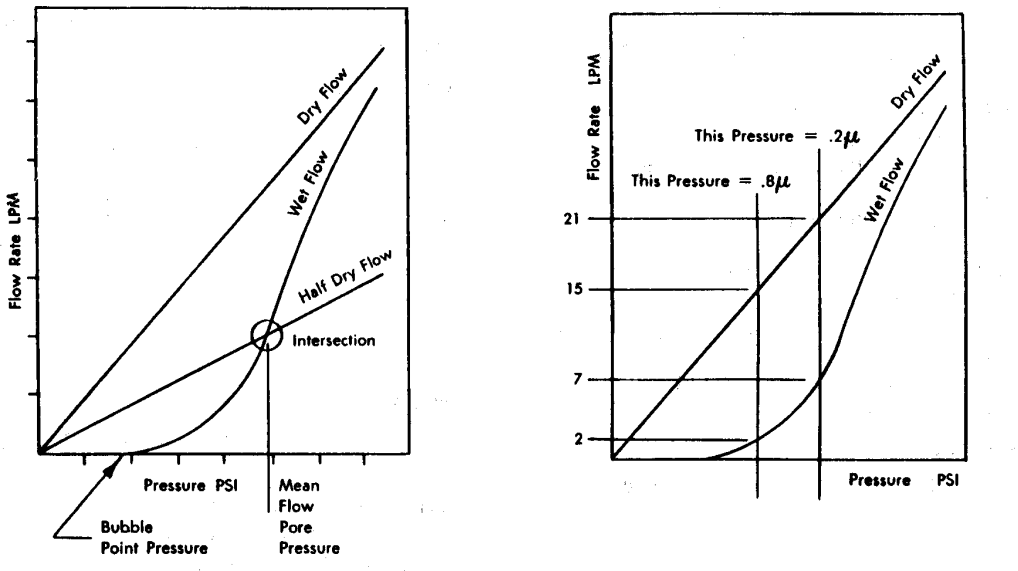

a) b)

Figure 7. The flow curves obtained by flow pore test a) and determination of the flow pore size distribution b) [94].

Ethanol was used as the wetting liquid due to its low surface tension 22 mN/m which allows measurement at rather low pressures. The low surface tension of ethanol also ensures good wetting and therefore wetting angle 0° was used in calculations. The flow pore test measures the narrowest opening of the pore capillary through the membrane and therefore differs from the Hg-porosimetry. The distribution of the narrowest openings however describes well the sieving properties of the membrane.

Permeability of the films was measured with de-ionised water. The free-standing sample was attached between seals at the bottom of the measuring chamber. The chamber was filled with de-ionised water and pressurised. Pressure was kept steady for several minutes and the permeate was collected. The permeability was calculated from the amount of permeate, the pressure difference, the membrane area, the

membrane thickness, collection time and the viscosity of the water. Permeability of the supported films was determined in two steps. The permeability of the substrate without the film and with the film was measured. The pressure drop over two-layered structure was assumed to be due to the pressure drops of both layers. Since the flux through the substrate and the membrane is the same, and the permeability of the substrate is known, the pressure drop over the substrate can be calculated. When the pressure drop over the substrate is subtracted from the pressure difference over the whole structure, the pressure drop over the membrane is obtained. Since the flux through the membrane was measured and the pressure drop over the membrane was calculated, the permeability of the membrane layer is obtained by using the membrane thickness and the viscosity of the water.

Hardness of the free-standing and the supported films was measured by Vickers indentation method with the load of 0.5 kg. The low load was selected in order to avoid the penetration through the membrane layer. The hardness value was calculated as the average of 10 measurements.

The morphology of powders and final membranes were characterized by transmission electron microscope (TEM) and scanning electron microscope (SEM). Microscopy studies were used for membrane thickness measurements, grain size measurements and for membrane pore morphology studies. The surface and cross-section of final membrane films were examined. The samples of cross-section were cast in polymeric resin disks followed by polishing and cleaning before examination. The grain size of membranes was measured from the surface micrographs by measuring at least 100 grains.

6 RESULTS AND DISCUSSION

The detailed results of the membrane preparation studies and functional properties are presented in Papers I-V. The filtration tests done with prepared membranes are presented at paper VI. The results of membrane preparation consist of two main categories: (1) the dip-coating of the membrane layer and (2) the sintering of the membranes. The sintering results are divided into subtitles, densification and evolution of the functional properties.

6.1 Dip-coating of membranes

The dip-coating of membrane layer is divided into subtitles, capillary absorption, layer growth mechanism and the effect of colloidal processing on the membrane layer growth.

6.1.1 Capillary absorption

The solvent with the substrate pore size defines the capillary pressure, which is the driving force of the dip-coating. The solvent composition affects the surface tension and the wetting angle between solvent and pore wall therefore having a twofold effect on the capillary pressure [II]. The liquid phase of the suspension also creates viscous drag in the pores of the substrate and hinders the absorption rate.

A model for calculation of the capillary pressure from the absorption of liquid into two-layered porous substrate was derived. The membrane is usually coated onto a two- or multi-layered substrate and so the capillary absorption also occurs into multi-layered structure. The absorption into the two-layered substrate is schematically presented in Figure 8.

The thin top-layer layer is filled first with square root relation to time. The filling is fast due to high capillary pressure created in the small pores. The coarse layer is filled with lower capillary pressure created in the coarse pores. The thin layer causes constant pressure drop during absorption while the pressure drop over the coarse pore sized structure is negligible.

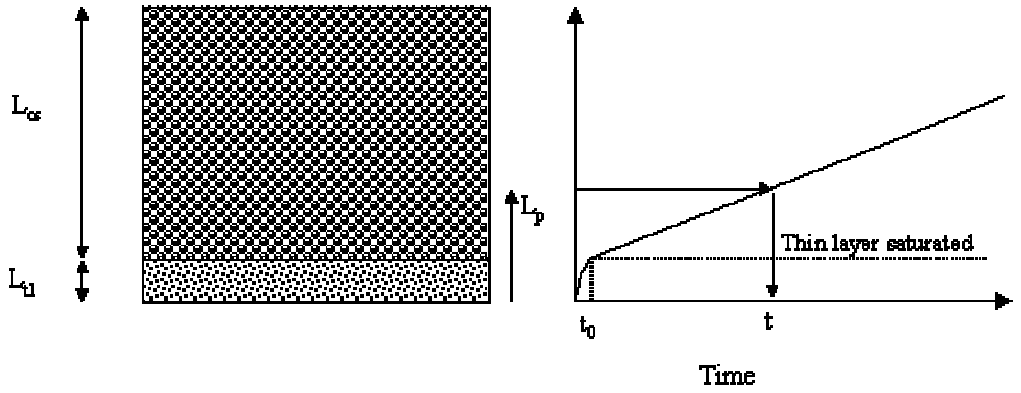

Figure 8. Absorption of liquid into asymmetric structure, when permeability of coarse structure is significantly higher compared with thin top layer [II].

The capillary pressure, ΔP_c, can be solved from the impregnation rate by equation

$$\Delta P_c = \left(\frac{\eta L_{tl}}{(1-\phi) K_{tl}} \right) \frac{L_p}{t} \tag{6}$$

Where K_{tl} is the permeability of the fine top layer, η is the viscosity of liquid phase, L_{tl} is thickness of fine pore sized top layer, ϕ is the volume fraction of solids in the coarse pore sized structure, L_p is the penetration depth and t is time. The penetration depth is a linear function of time. The capillary pressure can be calculated from the absorption rate when the properties of the thin top-layer and liquid are known.

The capillary pressure can be expressed also by Laplace equation, which gives the relation of capillary pressure to pore radius, R_p, wetting angle, θ, and surface tension, γ_{lv}

$$\Delta P_c = \frac{2\gamma_{lv} \cos\theta}{R_p} \qquad \Rightarrow \qquad \cos\theta = \frac{\Delta P_c R_p}{2\gamma_{lv}} \tag{7}$$

The surface tension of the liquid is related by the Young equation to solid-vapour interfacial energy, γ_{sv}, and solid-liquid interfacial energy γ_{sl}.

$$\gamma_{lv} \cos\theta = \gamma_{sv} - \gamma_{sl} \quad (8)$$

When the capillary pressure is plotted versus the surface tension of probe liquids the behaviour of wetting angle can be studied.

The capillary absorption was studied for solutions with different concentrations of sodium poly(methacrylic acid)(Na-PMAA), commonly used as dispersion agent, and poly(vinyl alcohol) (PVA) frequently used as a binder. The surface tensions, penetration rates, capillary pressures and wetting angles for different additive concentrations are presented in Table 1.

Table 1. Effect of additives on solution properties and capillary absorption

Solution	Dynamic viscosity [mPas]	Surface tension [mN/m]	L_p/t [m/s]	P_c [10^3 Pa]	cosθ
deionized water	0.84	72	$1.3 \cdot 10^{-4}$	5.8	0.71
0.5 g Na-PMAA/100 g H_2O	1.17	68.6	$9.3 \cdot 10^{-5}$	6.0	0.76
1 g Na-PMAA/100 g H_2O	1.32	67.8	$7.8 \cdot 10^{-5}$	5.7	0.73
2 g Na-PMAA/100 g H_2O	1.61	67.1	$7.0 \cdot 10^{-5}$	6.2	0.80
4 g Na-PMAA/100 g H_2O	2.14	64.7	$5.9 \cdot 10^{-5}$	7.0	0.94
8 g Na-PMAA/100 g H_2O	3.42	61.3	$3.8 \cdot 10^{-5}$	7.1	1.00
1 g PVA/100 g H_2O	1.25	48.6	$6.3 \cdot 10^{-5}$	4.3	0.78
2 g PVA/100 g H_2O	1.83	46.1	$3.8 \cdot 10^{-5}$	3.8	0.72
4 g PVA/100 g H_2O	3.68	45.4	$2.0 \cdot 10^{-5}$	4.0	0.77
8 g PVA/100 g H_2O	12.80	44.7	$4.3 \cdot 10^{-6}$	3.0	0.60

The addition of Na-PMAA increased viscosity less than the PVA addition. Na-PMAA decreased slightly the surface tension of the solution whereas PVA had a very strong reducing effect on the surface tension. The surface tension decrease of the PVA solution also resulted in a significant decrease in the capillary pressure. This decrease was not solely the result on the surface tension, while the wetting angle remained almost constant and therefore further decreased the capillary pressure [II].

In case of complete wetting, $\cos\theta = 1$, the capillary pressure increases with surface tension of liquid (solid straight line in Figure 9). When surface tension of liquid comes high enough, according to Young equation the wetting angle starts to increase, $\cos\theta < 1$. The result of incomplete wetting can be observed as a decrease of capillary

pressure (dashed curve in Figure 9), since decrease of cosθ is more significant than increase of surface tension of liquid. When surface tension of liquid increases further the wetting angle approaches 90 degrees and the capillary pressure disappears. With wetting higher than 90 degrees external pressure is needed for impregnation.

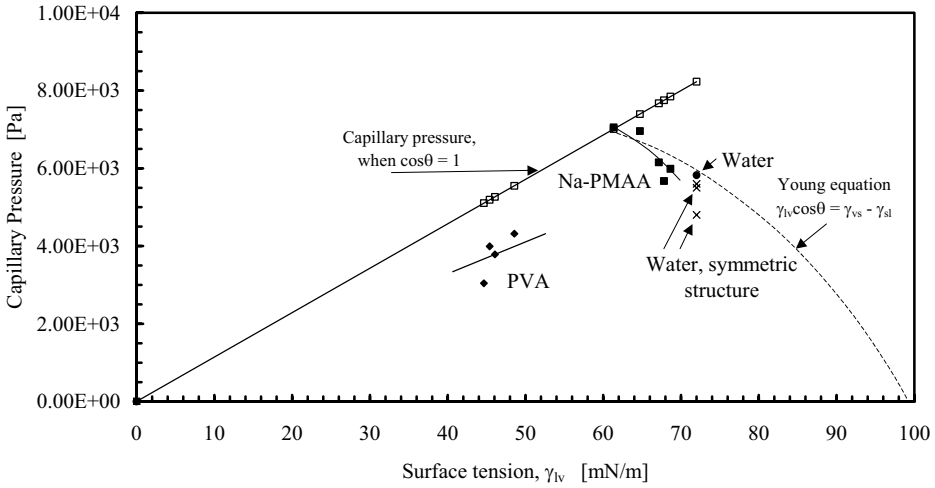

Figure 9. The calculated capillary pressures versus solution surface tensions. The straight line describes the capillary pressure dependence on surface tension with a wetting angle of 0° with different pore sizes. The dashed curve describes schematically the effect of the Young equation on the capillary pressure [II].

The Na-PMAA addition decreased surface tension and increased the capillary pressure as shown in Table 1 and Figure 9. The increase of the capillary pressure is related into improved wetting and is in accordance with behaviour predicted by the Young equation. The PVA addition did not follow the Young equation and the capillary pressure decreased significantly. The decrease of capillary pressure is partly related to decrease of surface tension, but as Table 1 shows the cosine of wetting angle is lower than predicted by the Young equation. The Young equation suggest complete wetting, cosθ = 1, but the calculated values are in range from 0.78 to 0.60 corresponding the wetting between water and pore walls. The PVA is a non-ionic molecule having low affinity on a hydrophilic surface and therefore the adsorption on the oxide surface is low. The advancing meniscus in the substrate pores does not

allow the PVA to adsorb onto the pore walls and liquid-vapour interface and therefore the wetting angle corresponds to the wetting angle of water [II].

The absorption that results in a two-layered substrate suggests that the frequently used assumption of the complete wetting between pore surface and slip solution may be erroneous. The additives used for slip preparation have different effects on the wetting angle and therefore on the capillary pressure. The adsorption behaviour of the additives can cause the deviation of wetting angle from that predicted by the Young equation. The polymer with low affinity on the oxide surface adsorbs slowly on the liquid interfaces and therefore the measured capillary pressure is smaller than that predicted by the Laplace and Young equations. The polymer with high affinity on the oxide surface adsorbs so fast on the liquid interface that the equilibrium equations of Laplace and Young are valid.

6.1.2 Layer growth and permeability evaluation

The dip-coated layer properties are dependent on the powder and solution properties, stage of the deflocculation and the slip parameters such as solid content, additive system, additive concentration and capillary pressure.

A model of solution absorption into two-layered substrate was further developed for modelling of the layer growth during dip-coating and for evaluation of the membrane layer permeability, K_{c2}, during dip-coating [III]. The model was developed based on the assumptions that the external fluid velocity, dL/dt, is same in all layers:

$$\eta \frac{dL}{dt} = \frac{K_{c2}}{L_{c2}} \Delta P_{c2} = \frac{K_{c1}}{L_{c1}} \Delta P_{c1} = \frac{K_{il}}{L_{il}} \Delta P_{il} = \frac{K_{cs}}{L_{pcs}} \Delta P_{cs} \qquad (9)$$

Where K_{c2}, K_{c1}, K_{il} and K_{cs} are the permeabilities of the growing layer, the layer formed after intermediate layer filling, the intermediate layer, and the coarse substrate structure. The layers are schematically presented in Figure 10. The permeability of the growing layer, K_{c2}, is defined to have different value than permeability during stage 1, K_{c1}, since the driving pressure is different. The pressure drops of respective layers are

ΔP_{c2}, ΔP_{c1}, ΔP_{il}, and ΔP_{cs}. L_{c2} is the thickness of the growing layer. L_{c1} is the thickness of the layer formed during Stage 1. L_{il} is the thickness of the intermediate layer, and L_{pcs} is the penetration depth of filtrate into the coarse substrate structure.

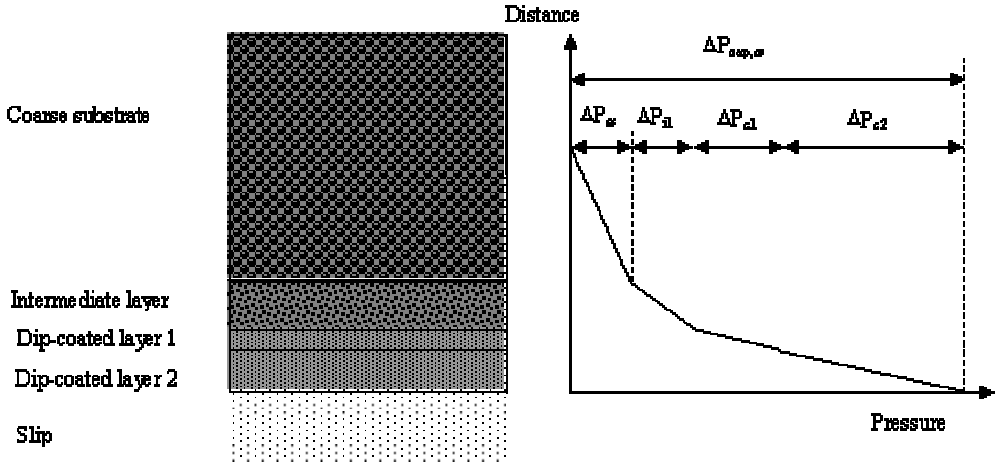

Figure 10. Schematic presentation of membrane layer build-up and pressure equilibrium [III].

As illustrated in Figure 10, the pressure equilibrium of the system can be expressed with the capillary pressure created by the coarse substrate structure, $\Delta P_{cap,cs}$, and the pressure drops caused by each layer:

$$\Delta P_{cap,cs} = \Delta P_{c2} + \Delta P_{c1} + \Delta P_{il} + \Delta P_{cs} \tag{10}$$

When volume balance is taken into account the layer thickness can be solved:

$$L_{c2} = \frac{B \pm \sqrt{B^2 - 4AC(t_2 - t_1)}}{2A} \tag{11}$$

Where:

$$A = \left[\frac{(\varphi_{c2}/\varphi_0 - 1)}{2K_{c2}} + \frac{(\varphi_{c2}/\varphi_0 - 1)^2}{2\varepsilon_{cs}K_{cs}} \right]$$

$$B = \left[\frac{(\varphi_{c2}/\varphi_0 - 1)L_{c1}}{K_{c1}} + \frac{(\varphi_{c2}/\varphi_o - 1)L_{il}}{K_{il}} \right]$$

$$C = \left[\frac{\Delta P_{cap,cs}}{\eta} \right]$$

Where coarse substrate porosity is ε_{cs}, growing layer solid fraction is φ_{c2}, slip solid fraction is φ_0 and the viscosity of the liquid phase is η. The negative solution is imaginary and can be therefore neglected. According to the solution the layer thickness is proportional to square root of time and dependent on the properties of the substrate structure and the layer itself. By using regression analysis the coefficients of Equation (11) can be calculated from the layer growth data. Coefficient A can be used further for calculation of membrane layer permeability:

$$K_{c2} = \frac{\left(\varphi_{c2}/\varphi_0 - 1\right)}{2\left(A - \frac{\left(\varphi_{c2}/\varphi_0 - 1\right)^2}{2\varepsilon_{cs}K_{cs}}\right)} \tag{12}$$

The model was used for the evaluation of membrane layer permeability for slips with and without PVA and Na-PMAA additions. The surface analysis of submicron, d_{50} ~ 0.5 μm, alumina powder showed Na and Si impurities. The potentiometric titration, dynamic mobility and dispersion stability measurements showed that these impurities on the alumina surface caused flocculation in pH range from 5 to 11, whereas more pure powder flocculated near isoelectric point at pH 8.8. These effects lead to the conclusion that in the electrostatic stabilization the pH should be adjusted below pH 5 [I]. The particle size of the slip with PVA was 250 nm, which was near the primary particle size observed with SEM and TEM. In slip with Na-PMAA the particle size was 370 nm, indicating a partly flocculated stage.

Figure 11 shows the porosity of layers cast from slips with different additive systems. No porosity gradient was found from layers dip-coated with different times. The layers made from electrostatically stabilized slips without additives had 45% porosity. A small addition of PVA increased the porosity of the layer up to 50%. Further additions of PVA did not increase the porosity significantly. The addition of Na-PMAA increased the porosity up to 60%. In the same way as PVA, the higher concentrations of Na-PMAA increased only slightly the porosity of the layers.

The growth of the cast layers is presented in Figure 12 with PVA addition and with Na-PMAA addition fitted with second order polynomials. The increase of PVA concentration gradually decreased the growth rate of the cast layer. The growth of layers cast from slips with Na-PMAA was significantly faster than the growth of the layers cast from slip without additives or slips with PVA addition.

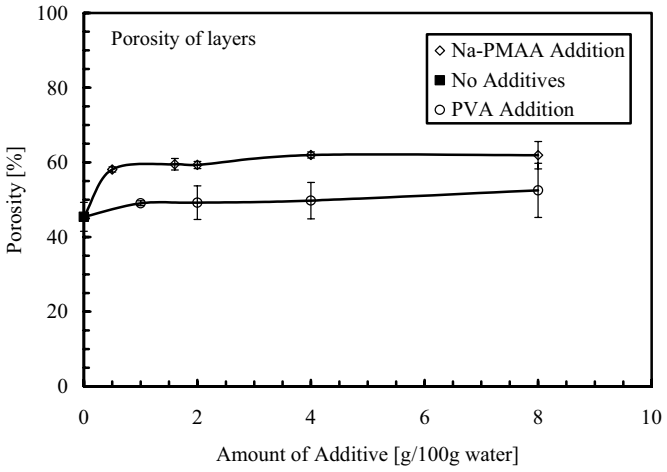

Figure 11. Porosity of the cast layers having different additive system. Error bars present the deviation of porosity values [II].

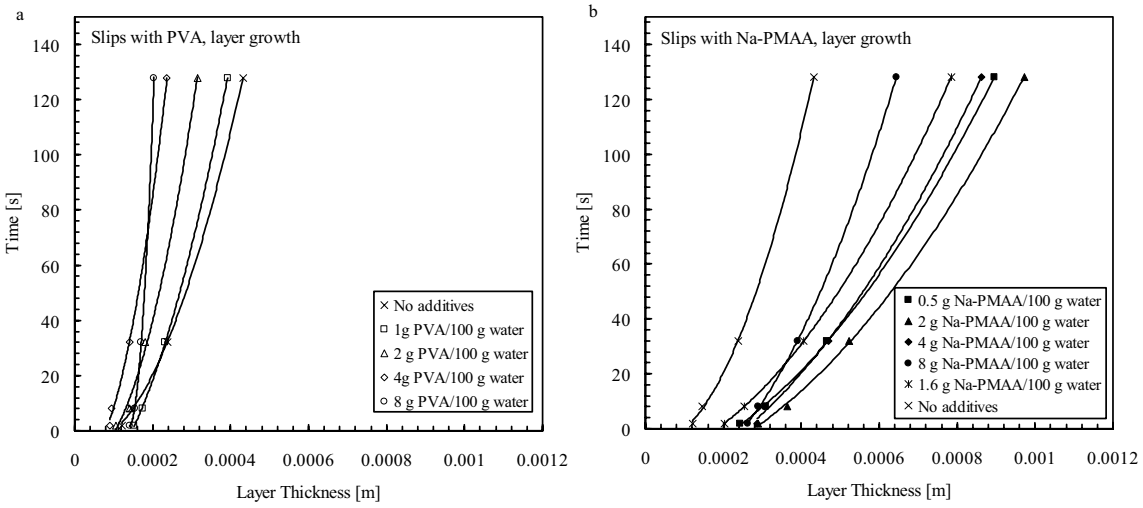

Figure 12. Build-up of layers with different additive systems fitted with second-order polynomial. Slips with a) PVA and b) Na-PMAA additions [III].

The permeability values were calculated with the model from coefficient A (Equations 11 and 12) by the fitted polynomials. Results are shown in Table 2. Permeability of layers dip-coated from slips containing PVA was slightly higher than permeability of layers prepared without additives. The increase of the PVA concentration did not change the permeability significantly. Use of Na-PMAA increased the permeability of dip-coated layer significantly.

Table 2. Permeability of dip-coated layers [II]

Solid load [% (v/v)]	Type of Additive	Amount of Additive [g/100 g water]	Measured Permeability [$10^{-16}m^2$]	Theoretical Permeability [$10^{-16}m^2$]
50	-	-	1.59	1.14
50	PVA	1	2.39	1.53
50	PVA	2	2.17	1.54
50	PVA	4	2.36/(2.51*)	1.62
50	PVA	8	1.20	2.03
50	Na-PMAA	0.5	7.65	3.36
45	Na-PMAA	1.6	9.31	3.84
50	Na-PMAA	2	10.50	3.78
50	Na-PMAA	4	9.03	4.89
50	Na-PMAA	8	5.59	4.86

* measured with water for sintered sample, 3 h at 1000°C.

Explanation for the difference between the measured and the theoretical permeability is the surface area used in the Kozeny-Carman Equation (1). The Kozeny-Carman equation uses the particle surface area for calculation of permeability. If the layer is packed from flocks instead of separate particles, the layer consists of larger capillaries between the flocks and smaller capillaries in the flocks. The flow is then through the larger capillaries rather than the smaller capillaries. The surface area in the Kozeny-Carman equation therefore should be the small surface area of flocks rather than the high surface area of separate particles. The difference between measured and theoretical permeability was the highest for slips with Na-PMAA addition. The pseudoplastic behaviour, larger particle size, and high porosity also confirm the presence of flocks in the slips with Na-PMAA. Since almost all the measured permeability values were higher than the theoretical values, flocks exist in all layers. The flock size is small in slips with PVA and in slips without additives.

The layer growth and permeability were also studied with flocculated slips. Flocculation was done by adjusting the pH near the isoelectric point or by creating high ionic strength in the solvent. The permeability calculated from the layer growth data also followed clearly the particle size as shown in Table 3.

Table 3. Effect of slip parameters on the permeability of dip-coated layers [IV]

Amount and Type of Additive [g/100 g water]	pH	Electrolyte	Particle Size [nm]	Porosity	Measured Permeability [$10^{-16}m^2$]
0.06 g PVA	4.4	-	230	32	3.11
0.24 g PVA	4.5	-	200	39	3.64
0.06 g PVA	9.8	-	420	35	23.20
0.24 g PVA	9.8	-	360	55	14.90
0.06 g Na-PMAA	9.3	-	520	48	4.73
0.06 g Na-PMAA	9.3	1 mM KCl	340	48	2.68
0.06 g Na-PMAA	9.2	100 mM KCl	430	53	8.96
0.06 g Na-PMAA	9.2	1 mM $CaCl_2$	330	52	2.77
0.06 g Na-PMAA	7.6	100 mM $CaCl_2$	5140	64	1710

The layers coated with the deflocculated PVA slips gave the lowest permeability values, which agrees with the low porosity and the smallest particle sizes. The layers from the flocculated PVA slips had very high permeability suggesting large flow channels between large flocks. Anyhow the voids caused by excess PVA cannot be clearly observed in permeability values especially in the case of flocculated slip having 2.15 wt-% PVA. The permeability of the layers prepared from the slips with Na-PMAA followed clearly the particle or flock size of the respective slip. This suggests that the flock size does not change during the layer growth by capillary compaction pressure and the flow channels between flocks are related to the flock size. With the low electrolyte concentrations the permeability of the coated layer varied within one order of magnitude being almost the same as the permeability of the deflocculated PVA slips. With the high electrolyte concentration, 100 mM $CaCl_2$, the permeability was 3 orders of magnitude higher than that of the deflocculated slips. The flocculated slip had very large particle size leading to high porosity and very high permeability of the coated layer. The very large particle size in slip with high concentration of divalent electrolyte suggests that dissociated Na-PMAA molecules may form divalent soaps and internal polymer bridging may lead formation of large and rather strong flocks.

6.1.3 Conclusions for dip-coating

A model for calculation of the capillary pressure for both symmetric and asymmetric structure was developed. The two-layered sample is suitable for studying the velocity dependence of the wetting angle since the constant penetration rate can be achieved. During the impregnation of the two-layered structure the thin low permeability top-layer creates a constant pressure difference. If the coarse pore-sized substrate has a high enough permeability the pressure drop created in it can be neglected.

The frequently used assumption of complete wetting may be erroneous. The additives used for slip preparation have a different effect on the wetting angle and therefore on the capillary pressure. The adsorption behaviour of the additives can cause deviation from wetting angle predicted by the Young equation.

PVA has a strong effect on the surface tension of the solution without effecting the wetting angle. The capillary pressure created by the PVA solution decreased considerably even at the low concentrations. According to the Young equation, the wetting should be improved when the surface tension decreases. The Young equation is the equilibrium equation and in the case of advancing meniscus the equilibrium is not achieved. The non-ionic PVA has a low affinity to the oxide surface, the adsorption is therefore slow. Due to incomplete wetting and the low surface tension of the PVA solutions the capillary pressure can be 15…40 % lower compared to the capillary pressure based on the assumption of the complete wetting.

The layer growth rate onto a two-layered substrate in dip-coating was modelled by using a second order polynomial. The coefficient of the second order term was used for the calculation of layer permeability. The permeability values calculated from the growth rate were higher than the theoretical permeability values predicted by the Kozeny-Carman permeability equation. The difference in permeability values was probably caused by the incomplete deflocculation of slips. The layers consist of flocks and the surface area used in calculation of theoretical permeability should be the area of the flocks, rather than the area of separate particles. The use of the particle surface area leads to too low permeability values, since the pore channels inside the flocks do not significantly participate into the fluid transport.

A correlation between colloidal state, particle size, porosity and permeability was observed. The pH, the amount and the type of the polymeric additive and the electrolyte concentration had a strong effect on the zeta potential and the particle size in the slip. The particle size of the slip governs the layer build-up rate during dip-coating and affects the porosity and permeability of the final layer. Small particle or flock size was obtained by using electrostatic stabilization and non-ionic PVA as the additive.

6.2 Sintering of membranes

The sintering behaviour and evolution of properties and microstructure of supported membranes were compared with those of free-standing films. The main interests were in densification, pore size, pore size distribution, permeability and hardness. The sintering studies focused on the membranes prepared with electrostatic deflocculation and with PVA addition, since this system resulted in the most uniformly packed layers. Three different powders were used for studying the effect of particle morphology and purity on the sintering behaviour.

6.2.1 Densification of supported and free-standing films

The free-standing films made from A 16 SG and CR 6 were sintered isothermally at temperatures of 1000°C, 1100°C, 1200°C and 1300°C. The shrinkage of the films was monitored with dilatometry in order to discover whether there exist differences in the densification behaviour between powders. According to models based on equal sized spherical particles, the power term of time, n in Equation (13) should be about 2/5 for solid state sintering [59]. Although the evaluation of the sintering mechanism based on the power term is unreliable it gives some information about the sintering kinetics.

$$\frac{\Delta L}{L} = \frac{h}{a} = ct^n \tag{13}$$

where $\Delta L/L$ is relative shrinkage, c and n constants and t is sintering time. Plots of $\log(l/l_0)$ versus $\log(t)$ are presented in Figure 13. The power terms of t for the films made from A 16 SG and sintered at temperatures of 1000°C, 1100°C, 1200°C and

1300°C were 0.21, 0.28, 0.14 and 0.18, respectively. The power terms of t for the films made from CR 6 powder were 0.22, 0.22, 0.30 and 0.58 for the same sintering temperatures. The deviation of power term of time from theoretical value of 0.4 shows that the isothermal densification was slower than the two-particle model predicts. Reasons for slower densification are the particle growth during sintering, the rearrangement of particles, the particle size distribution differs from mono-sized particles and the irregularities in particle shape. This deviation of the power term from the predicted value leads to the assumption that the microstructure also deviates from the structure predicted by the two-particle model.

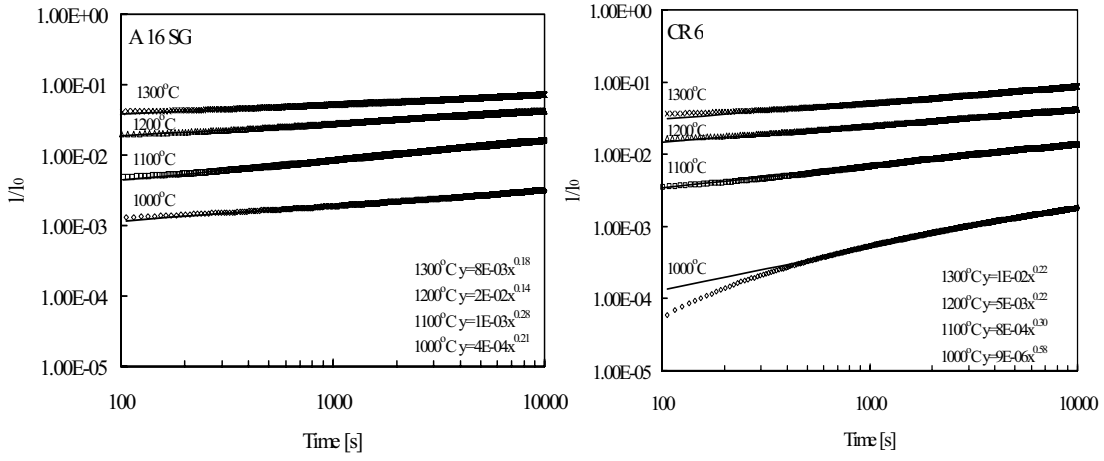

a) b)

Figure 13. Isothermal linear shrinkage of the free-standing films, a) A16 SG and b) CR 6. Lines present the fit of the power function given in legend [V].

The density of supported films was lower than that of the free-standing films as shown in Table 4.

Table 4. Density of the free-standing and the supported films after different sintering cycles [V].

	Density [g/cm^3]		
	A 16 SG	CR 6	AKP-30
	Free/supp.	Free/supp.	Free/supp.
Green	2.41/ n. a.	1.94/ n. a.	2.43/ n. a.
3 h 1000°C	2.43/2.02	1.95/1.65	2.50/2.51
3 h 1100°C	2.51/2.34	2.00/1.76	2.64/2.80
3 h 1200°C	2.73/2.18	2.10/1.64	2.90/2.67
3 h 1300°C	3.25/2.16	2.39/1.96	3.47/2.74
3 h 1400°C	3.79/2.34	2.51/1.93	3.85/2.41

The drying shrinkage of the thin films on the substrate is restricted leading to the lower density compared to the thick free-standing films, which are detached from the substrate during drying and can freely shrink in all three directions. The variation in green density of the free-standing films made from different powders indicates differences in packing behaviour during consolidation. The A 16 SG and AKP-30 films had rather dense packing. The free-standing CR 6 film had low green density, which suggests packing of agglomerates. Densification of the free-standing films during isothermal sintering was rather slow until the temperature was raised to 1300°C. The density of the supported films remained low after sintering at high temperatures. The densification of the supported films will probably occur at the higher temperatures and longer dwell times.

The specific surface area was compared with the fraction of theoretical density for evaluation of the densification mechanism. In Figure 14 one can be see that the specific surface area of the compacts decreased without densification at low temperatures indicating neck growth between particles by the surface diffusion mechanism or smoothening of particle surfaces.

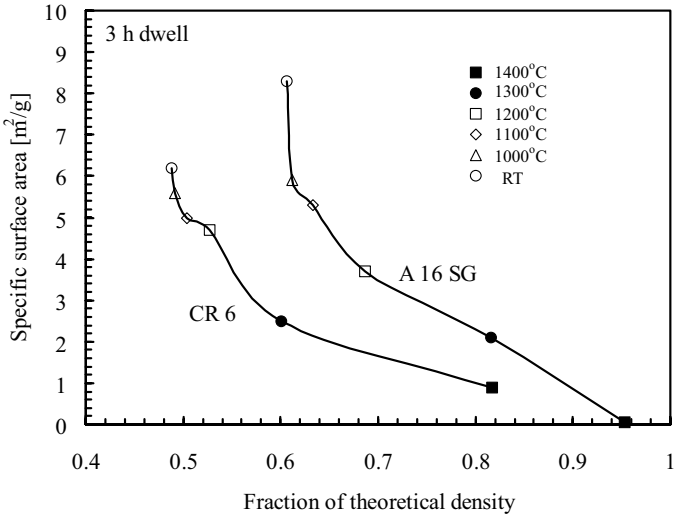

Figure 14. Specific surface area of the free-standing films versus the fraction of theoretical density [V].

At temperature ranges from 1000°C to 1100°C for A 16 SG and 1100°C to 1200°C for CR 6 the densification occurred fast when compared with the surface area reduction. Further increase of temperature led to fast reduction of the surface area. The fast reduction of surface area might be due to grain growth or local densification, since both mechanisms have minor effect on the macroscopic volume of the sample. At higher temperatures, 1200°C and over for A 16 SG and 1300°C and over for CR 6, the surface area decreased while compact density increased.

The grain size remained almost unchanged to sintering temperature of 1200^{o}C. Grain size coarsening occurred at higher temperatures. Sintering at 1400^{o}C resulted in the grain size three times larger than the original size. Examples of sintered microstructures for free standing and supported membranes sintered at different temperatures are shown in Figure 15.

There was no significant difference between grain sizes of the free-standing and the supported membranes. The slightly larger grain size of the supported membrane is probably resulting from the dip-coating method. Grain size coarsening alone does not explain completely the loss of surface area without densification. Some loss of surface area must be due to local densification of agglomerates, which do not significantly affect the sample volume.

Hardness of the free-standing films increased continuously when the sintering temperature was increased as shown in the inset table in Figure 16. The hardness values of the free-standing films were found to be dependent on the density of the film as shown in Figure 16. The hardness values of the free-standing films fall into the same density versus hardness curve for all films. When the supported films were sintered at low temperatures, the density increased without having an effect on the hardness. Sintering at higher temperatures increased the hardness, but did not have an effect on the density. After sintering at 1400°C the supported films had much higher hardness values compared to the free-standing films with the same density. Local densification does not affect the density, but increases the hardness and indicates that the bonds between the densified areas are also strong.

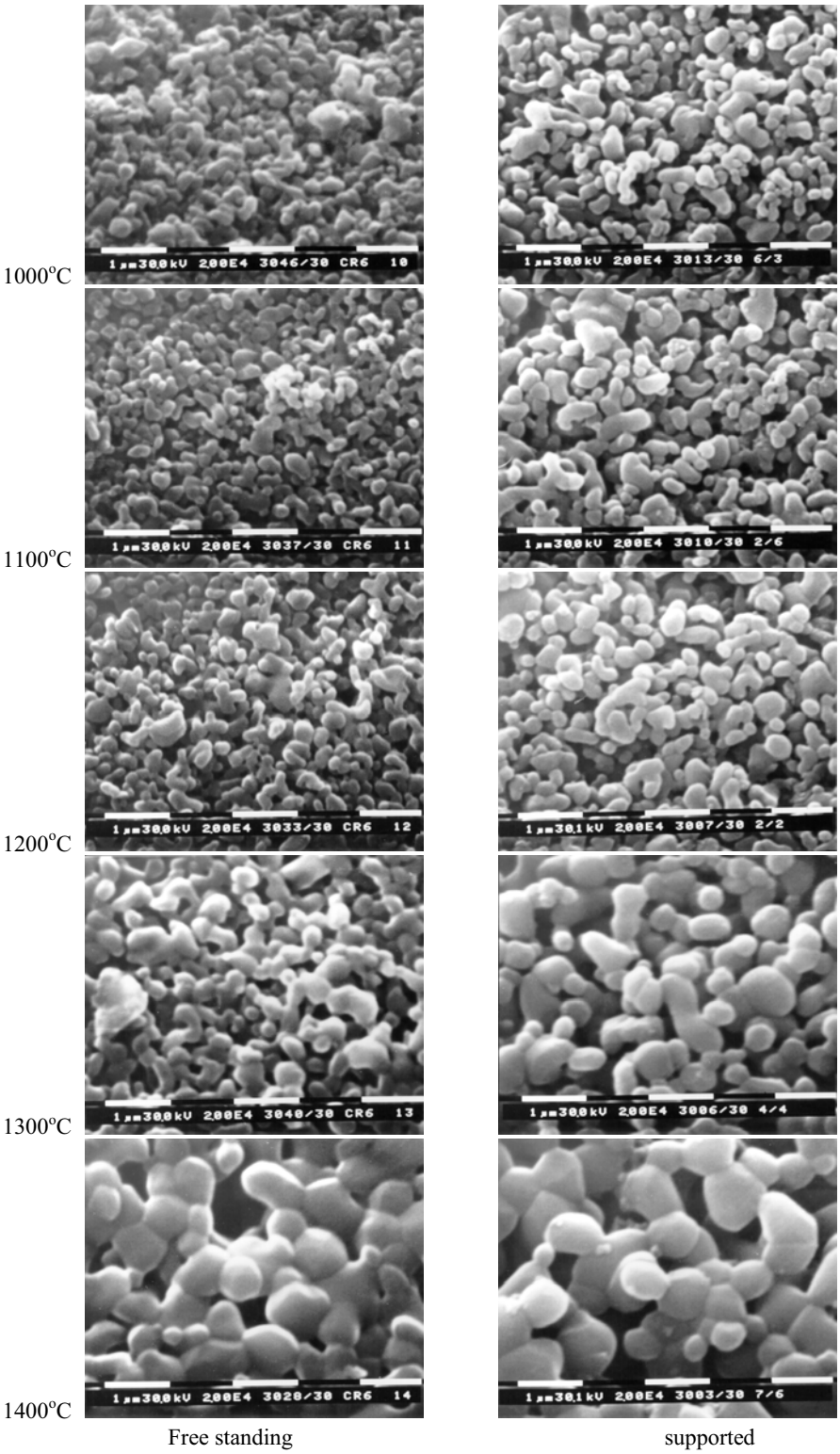

Figure 15. Surface structure of the free-standing and the supported CR 6 films sintered at different temperatures for 3 hours.

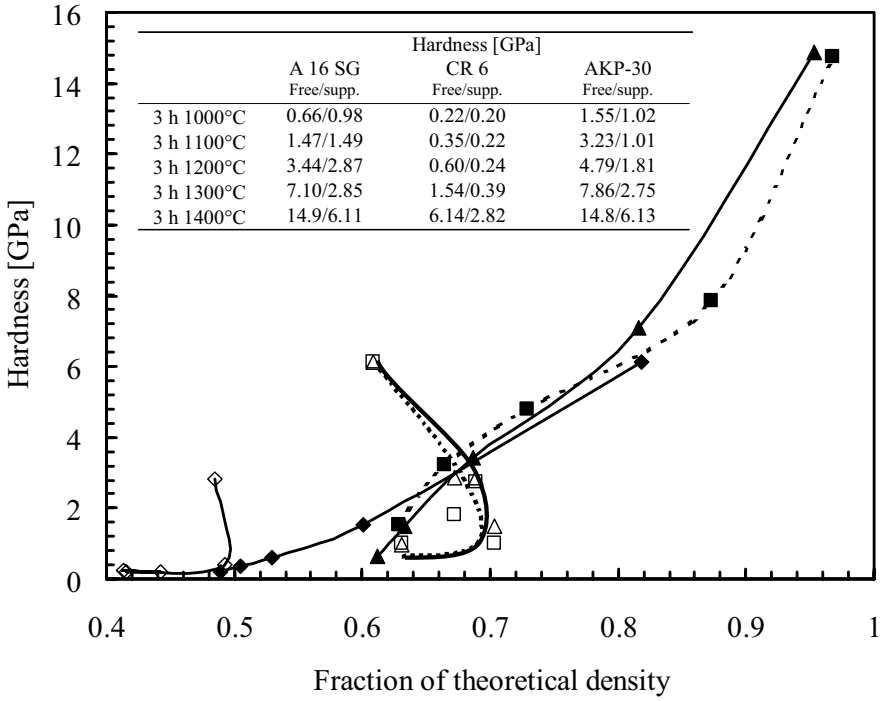

Hardness [GPa]	A 16 SG Free/supp.	CR 6 Free/supp.	AKP-30 Free/supp.
3 h 1000°C	0.66/0.98	0.22/0.20	1.55/1.02
3 h 1100°C	1.47/1.49	0.35/0.22	3.23/1.01
3 h 1200°C	3.44/2.87	0.60/0.24	4.79/1.81
3 h 1300°C	7.10/2.85	1.54/0.39	7.86/2.75
3 h 1400°C	14.9/6.11	6.14/2.82	14.8/6.13

Figure 16. Hardness of films compared with the fraction of theoretical density [V].

6.2.2 Evolution of functional properties

The sintering temperature had a strong effect on the pore size, pore size distribution and permeability. Increase in sintering temperature enlarges the pore size, broadens the pore size distribution and increases the permeability of supported membranes. The permeability of the free-standing films decreases after sintering at temperatures where significant densification occurs. The sintering temperature also had an effect on the flow channel geometry that will be also discussed more detailed in 6.2.3.

The mean pore sizes of the free-standing films remained almost the same after sintering at different temperatures as shown in Figure 17. The constant pore size suggests that the sintering proceeds mainly by the particle approach and neck growth, which reduces the surface area instead of coarsening of the pores.

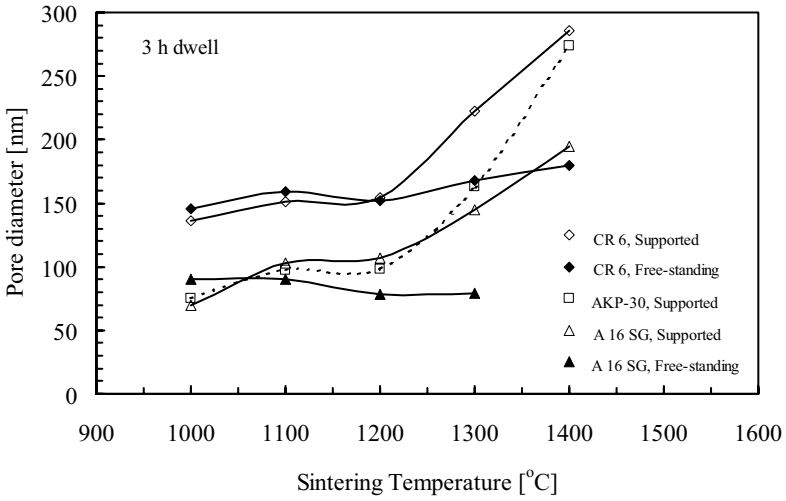

Figure 17.Mean pore diameter of the free-standing and the supported membranes [V].

The mean pore sizes of the supported films were the same as the pore sizes of the free-standing films when sintered at low temperatures, although the characterisation methods were different. The mean pore sizes of the supported films increased significantly after sintering at 1300°C and 1400°C. The pore growth occurred at temperatures where the strong densification of the free-standing films was observed. This suggests pore coarsening instead of densification since the porosity of the supported films decreased only slightly.

The pore size distributions of the supported films remained narrow after sintering at low temperatures. The distributions are presented in Figure 18 with the ratio, d_5/d_{50}, which describes the width of distribution.

The pore size distribution was narrow and monomodal for all the films sintered at the low temperatures. The broadening of pore size distribution was found after sintering at temperatures of 1300°C and 1400°C. The mean flow pore size increased indicating coarsening, but the significant, large pore size fraction also appeared and changed the size distribution to bimodal. The change of distribution from monomodal to bimodal occurred at the sintering temperatures where intense densification should occur. The

distribution broadening suggests that the film consists of areas where pores grow faster than in the other areas. Since the densification of the supported films was small, the large pores probably appear around the locally densifying particle agglomerates. If the pore size coarsening is related only to the grain growth, the shape of the distribution curve should remain constant without the presence of the fraction of very large pores. The pore size distributions of the supported A 16 SG and AKP-30 films broadened more clearly than the supported CR 6 film, since free-standing A16 SG and AKP-30 films densified at lower temperatures than the free-standing CR 6 film.

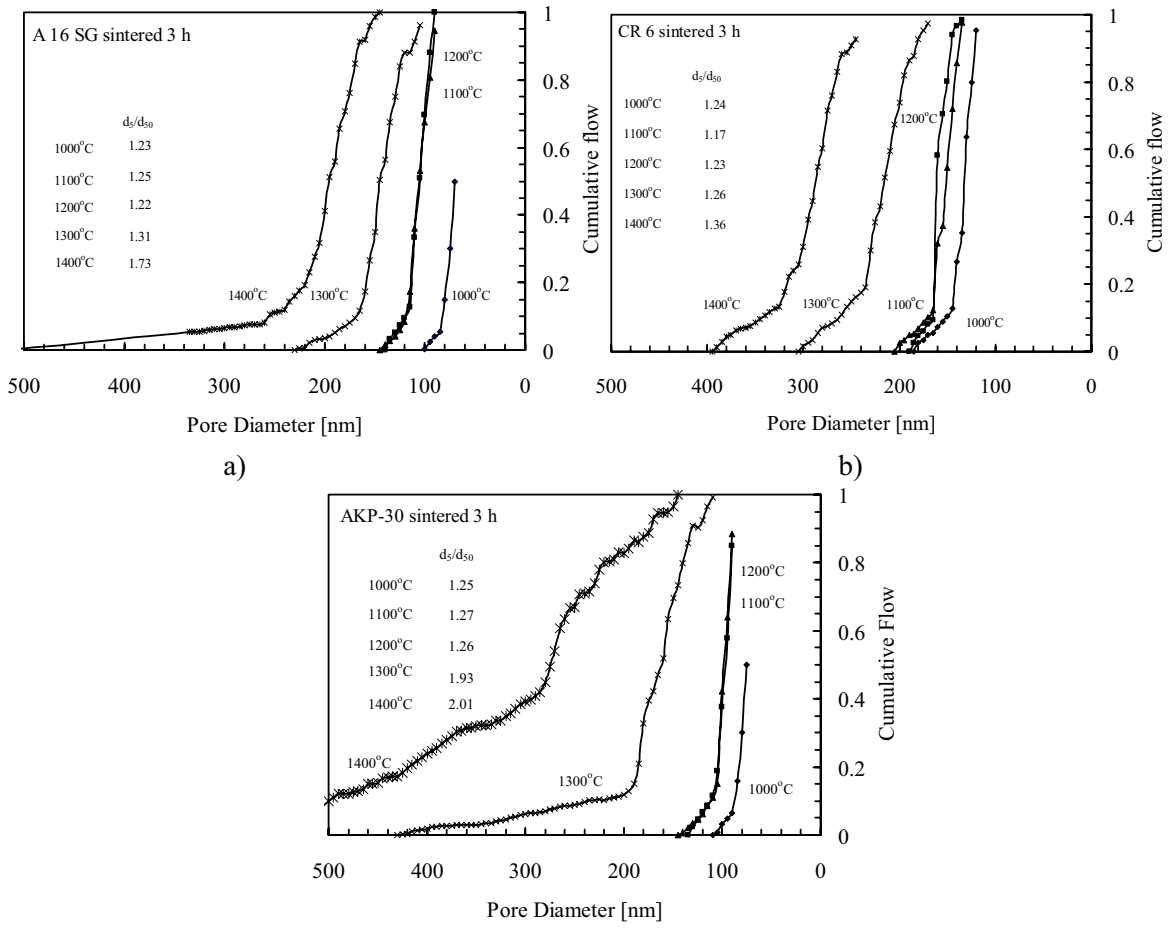

Figure 18. The flow pore diameter distributions of the supported membranes sintered at different temperatures. The ratio d_5/d_{50} is 5 % flow of wet sample compared with mean flow. Ratio describes the broadening of the pore size distribution: a) A16 SG, b) CR 6 and c) AKP-30 [V].

The permeability of the CR 6 films sintered at low temperatures was almost ten times higher compared with the A 16 SG and AKP-30 films as shown in Figure 19. The high porosity and the large pore size of the CR 6 films resulted in high permeability. When the sintering temperature of the free-standing A 16 SG film was raised, the permeability decreased continuously due to loss of porosity. The free-standing CR 6 film retained the high permeability value up to the sintering temperature of 1300°C and above that temperature the permeability decreased due the significant loss of porosity.

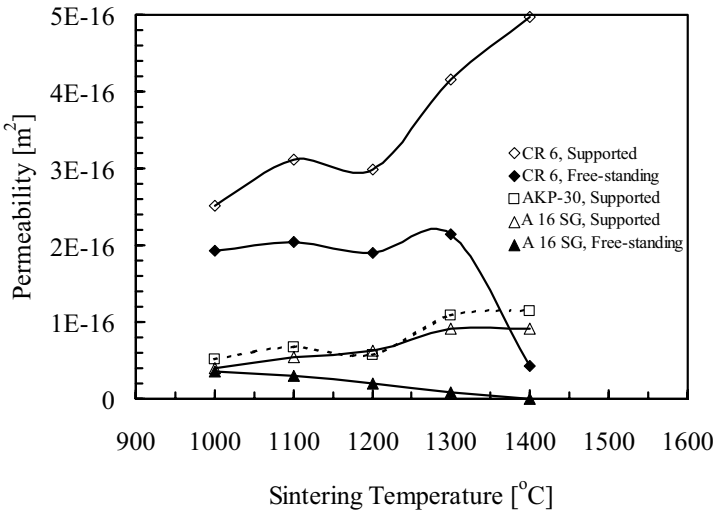

Figure 19. Permeability of films sintered for 3 h at different temperatures [V].

Permeability values of the supported films were close to values of the free-standing films made from the same powder after sintering at 1000°C, indicating rather similar flow channels as shown in Figure 19. When the sintering temperature was increased from 1000°C to 1200°C the permeability increased moderately, since there was neither significant change of pore size nor porosity. When the sintering temperature was raised to 1300°C and further to 1400°C there was more intense increase of permeability especially for the CR 6 film. This increase is related to the coarsening of

the pore size and the broadening of the pore size distribution. The A 16 SG and AKP-30 films had permeability increase when the sintering temperature was raised to 1300°C, but further rise in temperature did not change the permeability. The pore size of these films increased and porosity remained high, and so the reason for the steady permeability level after sintering at 1300°C and 1400°C must be in the pore geometry.

6.2.3 Evolution of pore morphology

The evolution of pore morphology during sintering can be evaluated from the permeability values by using the Kozeny-Carman flow Equation (1). Since the parameters of the Kozeny-Carman equation were measured for the free-standing films, the tortuosity factor k for these films can be calculated. The calculated values of k for the A 16 SG and CR 6 films are listed in Table 5. The k values for the both films were quite near each other after sintering at 1000°C, suggesting similar tortuosity and pore shape.

Table 5. Calculated Kozeny-Carman constant, k, values for the free-standing films [V]

	Kozeny-Carman constant k	
	A 16 SG	CR 6
3 h 1000°C	7.9	6.3
3 h 1100°C	9.5	4.8
3 h 1200°C	14.7	4.2
3 h 1300°C	16.4	3.3
3 h 1400°C	-	23

The higher initial k value for the free-standing A16 SG films is due to the broad particle size distribution and dense packing. The k values for the A 16 SG films increased continuously with the increasing sintering temperature, indicating that the flow path becomes more tortuous. The porosity of A 16 SG films decreased rapidly when the sintering temperature was increased, while pore size remained constant, leading to tortuous flow channels as described in A-case in the schematic presentation in Figure 20. The densification may also lead to a situation where the Kozeny-Carman flow equation is not valid. If dead end pores appear in the structure, these pores do not take part in the flow through the film. The measured surface area is therefore higher

than the surface area of the capillaries participating in the flow, resulting in too high calculated values of constant k.

The k values for the free-standing CR 6 films decreased when the sintering temperature was increased from 1000°C to 1300°C. The decrease of k suggests that the flow channels become less tortuous as presented in B-case in Figure 20. After sintering at 1400°C the k value increased significantly suggesting the formation of tortuous flow channels between dense agglomerates. Due to the low porosity of the membrane the closed-end pores however may appear in the structure leading to the high calculated value of the factor k.

The k factor of the supported films can not be directly calculated, since it is not possible to measure the specific surface area of the film on the substrate. The k factor can be evaluated by estimating the specific surface area of supported film based on the specific surface area of the free-standing film. After the sintering cycle the specific surface area of supported film is probably higher than that of free-standing film, due to higher porosity and difficulties in densification. The loss of surface area can be defined as $S_{BET/initial} - S_{BET/sintered}$. The loss of specific surface area for the supported films was taken to be from 1/2 to 1/5 of the loss of surface area for free-standing film. The k factors obtained with these surface area estimations are presented as dotted lines, case C, in Figure 20. The value of the k factor for supported films decreases continuously, indicating that the flow channels are straightening when the sintering temperature is raised. The straightening is the result of the restriction effect of the substrate. The dense agglomerates cannot approach each other, since shrinkage is allowed only in one direction perpendicular to surface. Therefore a much higher sintering temperature is needed before the flow channels transforms tortuous.

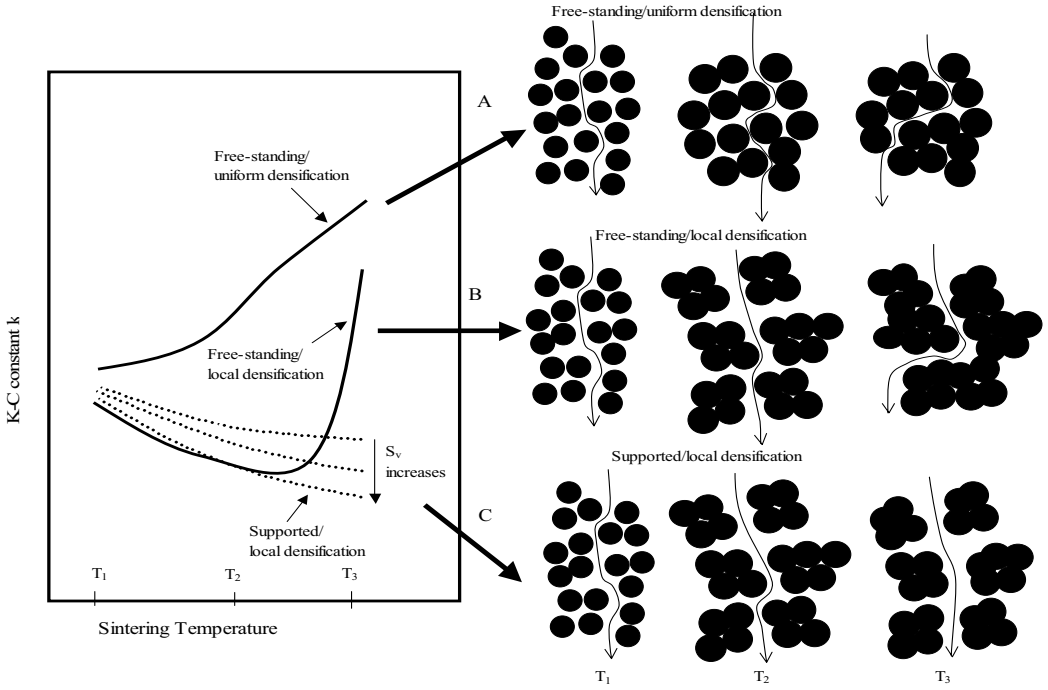

Figure 20. Evolution of the Kozeny-Carman constant k when increasing the sintering temperature for the free-standing and for the supported films. A) Uniform densification results in the increase of constant k, since the flow path becomes more tortuous. B) Local densification of the free-standing film decreases the value of k at low sintering temperatures due to straightening of the flow paths between densified areas. At the high sintering temperatures, the densification also occurs between agglomerates leading again to the tortuous flow paths. C) The rigid substrate prevents the densification between agglomerates resulting in the continuous decrease of the value of k and straightening of the flow channels between dense agglomerates. The densification of the supported film and the increased of value of k probably occurs at very high sintering temperatures[V].

The local densification was clearly observed from the polished cross-sections of the free-standing and the supported films as shown in Figure 21. The dense areas in the cross-section of the free-standing films were small in size and rather evenly distributed in the structure. The dense areas in the cross-section of the supported films were larger, and the low density areas were much looser as compared with those of

the free-standing films. The presence of the locally densified areas in the microstructure confirms the found difficulties in densification when the surface area and the theoretical density of the free-standing films was compared. The microstructural features found also confirm that the pore size coarsening and formation of large pores after sintering the supported films at high temperatures are the result of the local densification of the structure leading to low density areas with large pore size in between densified areas.

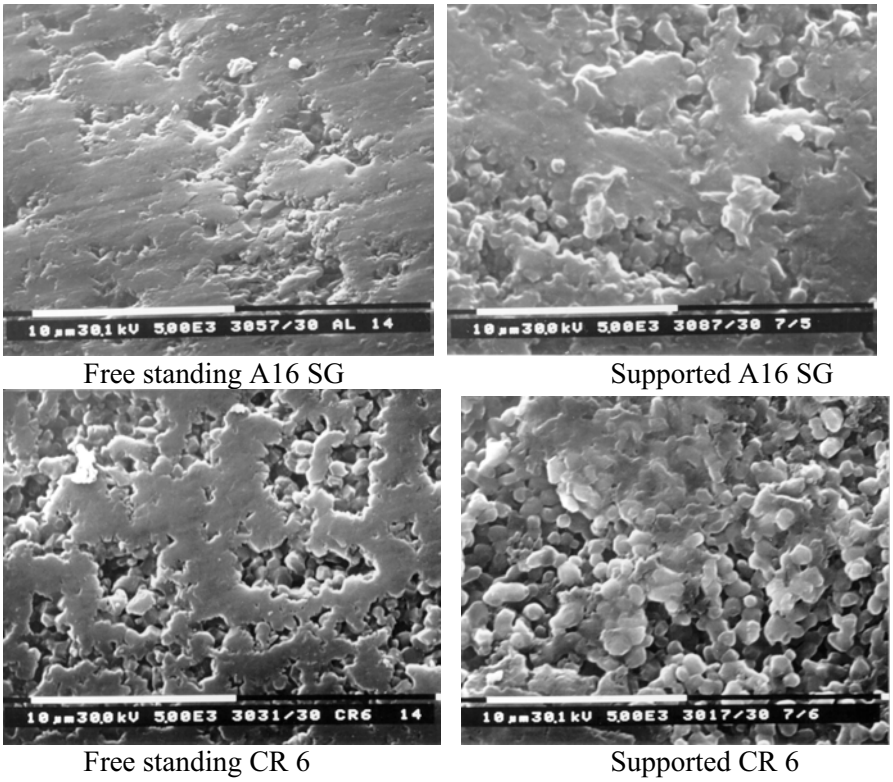

Figure 21. Polished cross sections of the free-standing and the supported films sintered for 3 h at 1400°C [V].

6.2.4 Conclusions for sintering

Sintering had a strong effect on the functional properties of the membrane. Sintering consolidates the structure and gives a required strength and hardness to the film but too high a sintering temperature may result in the loss of functional properties such as

narrow pore size distribution. The pore size coarsening is also significant at high sintering temperature.

Sintering at low temperatures, where shrinkage of the free-standing film is small, the narrow pore size distribution of the supported film is retained, but the strengthening of structure is small because of the narrow necks between the adjacent particles. The permeability is at the same level for the free-standing and the supported films.

Raising the sintering temperature to the range where moderate shrinkage occurs the restricted shrinkage of the supported film leads to the pore coarsening. The neck growth between the particles strengthens the structure, but hardness values are limited to one half of that of the free-standing films. The permeability of the supported films increase due to the pore growth.

Further increase of the sintering temperature results in the strong coarsening of the pore size of the supported films. The pore size distribution also changes from monomodal to bimodal. A fraction of very coarse pores develop in the structure. The rigid substrate restricts the shrinkage and leads to the local densification. The local densification also occurs in the free-standing films, but to a lesser extent. The effect of local densification on the microstructure, pore properties and hardness of the free-standing films is quite small. The local densification in the supported films leads to dense areas separated by the highly porous regions with large pores. The grain size measurements did not indicate faster grain growth in the supported films and the slower densification occurs therefore due to the local densification. The macroscopic densification remains negligible. The permeability of the supported films increase, but functionally the membrane has lost its sharp cut-off value. The hardness of the structure increases, but remains about half the value of the free-standing film.

Sintering studies showed that the uniform densification is very difficult to obtain. Minor deviations from homogenous packing such as loose agglomerates, particle size distribution etc. lead to non-uniform densification, that resulting in tortuous flow channels, large pore size and broad pore size distribution while the hardness and strength of the membrane layer remain low.

7 APPLICATIONS OF ALUMINA MEMBRANES

The strict requirements of non-polluting processes lead to evermore closed systems in industry. The use of porous ceramic semi-permeable films offers one solution especially for aggressive environments. The suitability of ceramic membranes for purification of paper industry wastewater was studied [VI, 96-101].

The porous ceramic structures were prepared and tested for several applications in corrosive environments and high temperatures at different fields of industry. In these applications the functionality of structures was tested as well as the durability at different environments. Structures were used for membrane filtration of wastewater, raw waters, oily waters, etc. For cleaning purposes resistance of the material against the ultrasonic treatment was improved and electron conductive surfaces were prepared. The applications and used structures are briefly described in this section. The alumina membranes were tested as prepared, with modified membrane surfaces and used as substrate structure for finer separation layers [102].

The alumina membranes were used in a pilot filtration apparatus for filtration tests of pulp and paper mill wastewater, stone cutting mine wastewater and arsenic removal from the dwell water [VI, 96-101]. Tests were done in collaboration with the Institute of Water and Environmental Engineering, Tampere University of Technology, Häme Regional Environment Centre (Pirkanmaa Regional Environmental Centre) and the Laboratory of Membrane Technology and Technical Polymer Chemistry, Lappeenranta University of Technology.

The quality of filtrate was found to be dependent on the pore size and the flow parameters. If the cross-flow velocity is too small the fouling layer is formed on the membrane surface. The filtration is done in the fouling layer, therefore the filtrate quality and flux are determined by the fouling layer. When the cross-flow rate is increased the shear stress on the surface increases and a fouling layer is not formed. Under this condition the filtrate quality and permeability are dependent on the membrane properties. Similarly, the effect of surface modification can be seen only when the shear on the surface is high enough. The used modifications: MgO, TiO_2 and SiO_2 were selected to change the charge of membrane surface. The results

suggested that industrial wastewater usually consist several compounds that may cause fouling of the membrane layer [VI]. Therefore it is very difficult to adjust the membrane surface charge so that fouling can be avoided. Feed has compounds that adsorb on negatively charged surfaces and compounds that adsorb on positively charged surfaces. The key factor seems to be how strong the adhesion of a certain compound on surface is and is it possible to remove the compound by shear, back flushing and cleaning procedures etc.

The ultrasonic treatment of the fouling layer requires mechanical durability of the membrane. Ultrasound produces cavitations which result in high local stresses on the surface and easily initiates damage to the membranes. The sintering cycle of the membrane was developed so that the membrane withstood the ultrasonic treatment. The resistance of the membrane against ultrasonic treatment was studied with VTT-Energy, Technical Research Centre of Finland.

The electronic conductive layers on the membrane were prepared for VTT-Energy. The conductive porous membranes were used as electrodes during filtration. The conductive layers of titanium nitride (TiN) were prepared by sputtering. The deposition parameters were selected so that conductivity was achieved without blocking the pores [103, 104].

The interaction between the alumina membranes and a corrosive environment was also studied [33, 34, 105]. Although the ceramic membranes are claimed to resist corrosive environments far better than other membrane materials, the high surface area and the open porous structure is sensitive to loss of mechanical properties even at low dissolution rates. The tests preformed with alumina membranes showed that the usual monitoring of weight loss alone does not clearly show the corrosion behaviour [34,105]. Weight loss combined with the monitoring of permeability, pore size, porosity and hardness provided much better information about the corrosion mechanism. Corrosion was found to concentrate on the grain boundaries between particles, where the lattice structure is distorted and impurities are concentrated. Even small corrosion rates on grain boundaries reduce the mechanical properties considerably. More specific information is obtained from the corrosion by monitoring

the amount of dissolved material in the corrosion media. Monitoring of dissolved material enables the detection of very small corrosion rates [34].

The alumina membranes were also used for testing the separation oil from water. Oil from water separation worked when the oil was in the form of an emulsion. The water went through the membrane leaving oil droplets on the other side.

8 CONCLUDING REMARKS

In this study the preparation cycle of the alumina ceramic membrane was characterized. The study consisted of raw material characterization and selection, colloidal processing with different additives, modelling of absorption in a multi-layer substrate and modelling of layer growth during dip coating, the effect of colloidal processing on growth kinetics, effect of sintering on functional properties such as pore size, pore morphology and permeability. Lastly, the performance of the prepared membranes was studied in different industrial processes.

The main result was that even membrane preparation is quite widely studied the effect of different preparation steps on final properties of membranes is incompletely characterized. The following key points were observed:

1. Effect of slip additives is not always straightforward. The additive system has an effect on the dip coating driving force, capillary pressure, in a way that does not always correspond to the equilibrium state.
2. Layer formation also depends on the substrate properties. When dip-coating with low solid content slips on multilayer substrate the effect of substrate must be included. The substrate has an effect on the capillary pressure and it may also have significant flow resistance.
3. Slip preparation or colloidal processing has the greatest effect on the layer formation kinetics. The layer growth rate and resulting layer properties can be largely varied with parameters of colloidal processing such as deflocculation stage, additive system solid load, etc.
4. The sintering mechanism of supported layer deviates from that of free standing films. At a temperature range were significant shrinkage of free standing films occurs, the supported films do not shrink, but instead the pore size increases. This is due to uneven shrinkage or local densification even in cases where the particles were completely deflocculated and densely packed.

The liquid phase has a significant effect on the layer growth in colloidal filtration based dip coating. Additives such as Na-PMAA and PVA have a strong effect on the viscosity, which is a commonly known fact. These additives also have an effect on the

capillary pressure created in the pores of the substrate. The capillary pressure is the driving force of colloidal filtration and it affects the layer growth kinetics. Na-PMAA addition decreases slightly the surface tension and simultaneously enhances the wetting according to the Young equation. This results in the increase of capillary pressure. PVA addition strongly reduces surface tension but does not have an effect on wetting behaviour. This results in a strong reduction of capillary pressure. Phenomenon is frequently neglected although it has a strong effect on layer growth rate. Accurate control of layer growth is usually needed and the use of PVA offers one solution to achieve thin membrane layers.

The colloidal processing is the major process step affecting the layer growth kinetics. Frequently used electrosteric stabilization of alumina with polyelectrolytes leaves small flocks in slip instead of complete dispersion. These flocks cause fast layer growth and difficulties in controlling of layer thickness. The resulting layer also has high porosity compared with layers dip coated from completely deflocculated slip. The particle or flock size of the slip correlated well with the growth kinetics, layer permeability and porosity. Electrostatic stabilization with pH control combined with PVA addition resulted in very small particle size indicating complete deflocculation. The layer porosity was smaller compared with Na-PMAA deflocculated slips. The concentration of PVA addition had no significant effect on the deflocculation, but had a strong effect on viscosity and capillary pressure. These findings resulted in slow and easy-to-control membrane layer growth during dip coating. The reduction of the slip solid content further reduced the layer growth rate.

The sintering studies showed that the supported structure behaves similar to the free standing structure at low sintering temperatures. At low sintering temperature consolidation occurs without particle centre approach and the restrictive substrate has no effect. At temperatures where significant shrinkage occurs the substrate restriction play an important role. The pore size grows, pore size distribution broadens and loss of porosity is very small due to restricted mass transport. The pore growth is not the result from grain size coarsening, but the local densification in supported film. Local densification occurs at flocks or areas with smaller particles or other higher density areas. The broadening of pore size distribution causes the loss of sharp cut-off value and therefore reduces membrane performance. The difficulties in densification

combined with pore size increase lead to higher permeability. The permeability increase is more pronounced due to the change of pore morphology. Local densification straightens the pore channels and reduces therefore the tortuosity factor. At low sintering temperatures the hardness of supported films is very low. The increase of sintering temperature has significant effect on the hardness only at very high temperatures where the pore size may have lost its sharp cut-off value. However, depending on applications, the loss of narrow pore size distribution may be acceptable if the hardness and mechanical properties are adequate.

The alumina membranes were tested at several applications. The filtration conditions were found to be the most important parameter both on separation, permeability and long-term performance. The membrane surface modifications have only minor effect on the membrane performance if the fouling layer can not be removed by cross-flow filtration conditions, mechanical arrangements, ultrasonic cleaning or back pulsing. These methods set the mechanical requirements of the membrane layer.

Finally, it must be noted that membrane preparation from a powder selection to filtration experiments is a vast area and it is obvious that this study was focused on only a few points of preparation field. During the study the attention has been laid on industrial fields, which have importance among the Finnish industry. These requirements had been as guidance when selecting the research areas among membrane preparation.

REFERENCES

1. H. Strathmann, Membrane Separation Processes: Current Relevance and Future Opportunities, AIChE Journal 47 (2001) 1077-1087.

2. A. J. Burggraaf and L. Cot, General overview, trends and prospects, pp 1-20 in *Fundamentals of Inorganic Membrane Science and Technology* (eds. A. J. Burggraaf and L. Cot) Elsevier Science B.V., Amsterdam, 1996.

3. M. Nyström and J. Nuorttila-Jokinen, Current Trends in Membrane Technology, Kemia-Kemi 23 (1996) 663-672.

4. K. Chan and A. Brownstein, Ceramic Membranes - Growth Prospects and Opportunities, American Ceramic Soc. Bulletin 70 (1991) 703-707.

5. M. Laatikainen, M. Lindström and M. Nyström, Kalvotekniset erotusmenetelmät 1980-luvulla. Osa 1: Mikrosuodatus, ultrasuodatus ja käänteisosmoosi, Kemia-Kemi (1986) 385-493 (In Finnish).

6. R.R. Bhave, Inorganic Membranes. Synthesis, Characteristics and Applications, Chapman & Hall, New York, 1991, 312 p

7. A. J. Burggraaf, Important characteristics of inorganic membranes, pp. 21-34 in *Fundamentals of Inorganic Membrane Science and Technology* (eds. A. J. Burggraaf and L. Cot) Elsevier Science B.V., Amsterdam, 1996.

8. A. Julbe, D. Farrusseng and C. Guzard, Porous Ceramic Membranes for Catalytic reactors – Overview and New Ideas, J. of Membrane Science 181 (2001) 3-20.

9. H. J. M. Bouwmeester and A. J. Burggraaf, Dence ceramic membranes for oxygen separation, pp. 435-528 in *Fundamentals of Inorganic Membrane Science and Technology* (eds. A. J. Burggraaf and L. Cot) Elsevier Science B.V., Amsterdam, 1996.

10. C. Leger, H De L. Lira and R. Paterson, Preparation and Properties of Surface Modified Ceramic Membranes. Part II. Gas and Liquid Permeabilities of 5 nm Alumina Membranes Modified by a Monolayer of Bound Polydimethylsiloxane (PDMS) Silicone Oil, Journal of Membrane Science, 120 (1996) 135-146.

11. E. Soterakou, K. Beltsios and N. Kanellopoulos, Asymmetric Ceramic Membranes from Langmuir-Blodgett Deposition Precursors: Deposition of Fatty Acid Salts on Porous Ceramic Substrates, Journal of the European Ceramic Society 20 (2000) 1105-1113.

12. A.W. Smith, Process for producing an anodic aluminium oxide membrane, 1974, U.S. Patent 3,850,762

13. R. Schnabel, Separation Membranes from Porous Glass and Method to Produce Them, 1976, German Patent 2,454,111,

14. K. H. Lee and S. J. Khang, A New Silicon-based Material Formed by Pyrolysis of Silicone Rubber and its Properties as a Membrane, Chem. Eng. Commun. 44 (1986) 121-132.

15. C. Guizard, Sol-Gel Chemistry and its Application to Porous Membrane Processing, pp. 227-258 in *Fundamentals of Inorganic Membrane Science and Technology* (eds. A. J. Burggraaf and L. Cot) Elsevier Science B.V., Amsterdam, 1996.

16. S. Vercauteren, K. Keizer, E. F. Vansant, J. Luyten and R Leysen, Porous Ceramic Membranes; Preparation, Transport Properties and Applications, J. of Porous Materials 5 (1998) 241-258.

17. P. M. Biesheuvel and H. Verweij, Design of Ceramic Supports: Permeability, Tensile Strength and Stress, J. of Membrane Science 156 (1999) 141-152.

18. A. Larbot, Ceramic Processing Techniques of Support Systems for Membrane Synthesis, pp. 119-140 in *Fundamentals of Inorganic Membrane Science and Technology* (eds. A. J. Burggraaf and L. Cot) Elsevier Science B.V., Amsterdam, 1996.

19. C. Simon, R. Berendsen, H. Raeder, M. Seiesten, A. Julbe, C. Monteil, I. Laazis, J. Etienne and L. Cot, Tape Casting of Flat Ceramic Membranes, Key Eng. Materials 61/62 (1991) 425.

20. B. C. Bonecamp, Preparation of Asymmetric, Ceramic membrane Supports by Dip-Coating, pp. 141-226 in *Fundamentals of Inorganic Membrane Science and Technology* (eds. A. J. Burggraaf and L. Cot) Elsevier Science B.V., Amsterdam, 1996.

21. K. A. DeFriend and A. R. Barron, A Simple Approach to Hierarchical Ceramic Ultrafiltration Membranes, J. of Membrane Science 212 (2003) 29-38.

22. J. Coronas and J. Santamaria, Separation Using Zeolite Membranes, Separation and Purification Methods 28 (1999) 127-177.

23. K. Linqvist and E. Linden. Preparation of Alumina Membranes by Tape Casting and Dip Coating, J. of the European Ceramic Society 17 (1996) 359-366.

24. K. Darcovitch, D. Roussel and F. N. Toll, Sintering Effects Related to Filtration Properties of Porous Continuously Gradient Ceramic Structures, J. of Membrane Science 183 (2001) 293-303.

25. K. Darcovitch, F. Toll, P. Hontanx, V. Roux and K. Shinagawa, An Experimental and Numerical Study of Particle Size Distribution Effects on the Sintering of Porous Ceramics, Materials Science and Engineering A348 (2003) 76-83.

26. D. Farrusseng, A. Julbe, M. Lopez and C. Guizard, Investigation of Sol-gel Methods for the Synthesis of VPO Membrane Materials Adapted to the Partial Oxidation of n-butane, Catalysis Today 56 (2000) 211-220.

27. Y. A. Ma, Adsorption Phenomena in Membrane Systems, pp 23-66 in *Fundamentals of Inorganic Membrane Science and Technology* (eds. A. J. Burggraaf and L. Cot) Elsevier Science B.V., Amsterdam, 1996.

28. A. Julbe and J. D. F. Ramsay, Methods for the Characterization of Porous Structure in Membrane Materials, pp. 67-118 in *Fundamentals of Inorganic Membrane Science and Technology* (eds. A. J. Burggraaf and L. Cot) Elsevier Science B.V., Amsterdam, 1996.

29. P. C. Carman, Fluid Flow Through Granular Beds. Trans. Inst. Chem. Eng. 15 (1937) 150.

30. A. F. M. Leenaars and A. J. Burggraaf, The Preparation and Characterization of Alumina Membranes with Ultra-fine Pores. Part 4. Ultrafiltration and Hyperfiltration Experiments, Journal of Membrane Science 24 (1985) 261-270.

31. J. Züter, Chemical and Thermal Stability of (Modified) Mesoporous Ceramic Membranes, PhD Thesis, University of Twente, Enschede, The Netherlands, 1995.

32. T. Van Gestel, C. Vandecsteele, A. Buekenhoudt, C. Dotremont, J. Luyten, R. Leysen, B Van der Bruggen and G. Maes, Alumina and Titania membranes for nanofiltration: Preparation, Characterization and Chemical Stability, Journal of Membrane Science 207 (2002) 73-89.

33. E. Levänen, T. Koiranen, A.-P. Nikkilä, L. Grönroos and T. Mäntylä, Static Corrosion of Alumina Membranes, The Second Nordic Seminar of Membranes, Materials and Processes, Oslo, Norway, April 18-19, 1996.

34. J. Laakso, Corrosion of Ceramic Membranes, Tampere University of Technology, Institute of Materials Science, M.Sc Thesis, 1997, 118 p. (in Finnish)

35. N. Das and H.S. Maiti, Effect of Size Distribution of the Starting Powder on the Pore Size and its Disribution of Tape Cast Alumina Microporous Membranes, J. of European Ceramic Society 19 (1999) 342-345.

36. R. M. German, *Particle Packing Characteristics*, Metal Powder industries Federation, Princeton, New Jersey, 1989, 443 p.

37. J. Zheng, W. B. Carlson and J. S. Reed, The Packing Density of Binary Powder Mixtures, Journal of the European Ceramic Society 15 (1995) 479-483.

38. J. A. Lewis, Colloidal Processing of Ceramics, Journal of American Ceramic Society 83 (2000) 2341-2359.

39. M. F. Yan, Solid State Sintering, pp. 635-669 in *Advances in Ceramics, Vol. 21, Ceramic Powder Science*, American Ceramic Society, 1987.

40. R. D. Bagley, I. B. Cutler and D. L. Johnson, Effect of TiO_2 on Initial Sintering of Al_2O_3, Journal of American Ceramic Society 53 (1970) 136-141.

41. J. W. Filbri, H. L. Schram and S. Sinnema, Sintering of Porous Alumina Using MnO and TiO_2, , pp. 257-264 in *Fourth Euro Ceramics: Basic Science – Developments in Processing of Advanced Ceramics –Part II*, (ed. C. Galassi), Vol. 2.

42. A. Aksay and J.Pask, Stable and Metastable Phase Equilibria in the System SiO_2-Al_2O_3. Journal of American Ceramic Society 45 (975) 507.

43. R. F. Hayden, Study of the Resistance of Refractories to Alkali Vapors, M.Sc Thesis, Virginia Polytechnic Institute, 1976.

44. J. W. Evans and L. C. De Jonghe, *The production of Inorganic Materials*, Maxwell Macmillan International Publishing Group, New York, Oxford, Singapore, Sydney, 1992, 541 p.

45. B. V. Derjaguin and L. D. Landau, Theory of Stability of Highly Charged Lyophobic Sols and Adhesion of Highly Charged Particles in Solution of Electrolytes, Acta Physicochim. URSS 14 (1941) 633-652.

46. E. J. W. Verwey and J. Th. G. Overbeek, *Theory of Stability of Lyophobic Colloids*, Elsevier, Amsterdam, The Netherlands, 1948.

47. J. N. Israelachvili, *Intermolecular and Surface Forces, with Applications to Colloidal and Biological Systems*, Academic Press, London, San Diego, New York, 1985.

48. A. Foissy, A. El Attar and J. M. Lamarche, Adsorption of polyacrylic acid on titanium dioxide, Journal of Colloid and Interface Science 96 (1989) 275-287.

49. J. Cesarano and I. H. Aksay, Processing of highly concentrated aqueous α-alumina suspensions stabilized with polyelectrolytes, Journal of the American Ceramic Society 71 (1988) 1062-67.

50. F. Nunes, A. G. Lamas, M. Almeida and H. M. M. Diz, Influence of deflocculants on the characteristics of alumina bodies obtained by slip casting, Journal of Materials Science 27 (1992) 6662-6666.

51. J. Cesarano, I. H. Aksay and A. Bleier, Stability of aqueous α-alumina suspensions with poly(metacrylic acid) polyelectrolyte, Journal of the American Ceramic Society 71 (1988) 250-55.

52. R. Arnold and J. Th. G. Overbeek, The dissociation and specific viscosity of poly(methacrylic acid), Rec. Trav. Chim. Pays-Bas 69 (1950) 192-206.

53. J. Papenhuijzen, H. A. Van der Schee and G. J. Fleer, Polyelectrolyte Adsorption I. A New Lattice Theory, Journal of Colloid and Interface Science 104 (1985) 540-61.

54. R. Moreno, The Role of Slip Additives in Tape Casting Technology: Part II – Binders and Plasticizers, American Ceramic Society Bulletin 71 (1992) 1647-1657.

55. A. Kristoffersson, Water-based Tape Casting of Ceramics and Fabrication of Ceramic Laminates, PhD Thesis, Chalmers University of Technology, Göteborg, Sweden, 1999.

56. P. C. Hidber, T. J. Graule and L. J. Gauckler, Competitive adsorption of citric acid and poly(vinyl alcohol) onto alumina and its influence on the binder migration during drying, Journal of the American Ceramic Society, 78 (1995) 1775-80.

57. B. E. Platonov, A. A. Baran and T. A. Polischuk, Adsorption of poly(vinyl alcohol) and its effect on the electrosurface characteristics of some oxides, Acta Phys. Chem. 25 (1979) 201-208.

58. C. S. Khadilkar and M. D. Sacks, Effect of poly(vinyl alcohol) on the properties of model silica suspensions, pp 397-409 in *Ceramics Transactions, Vol 1, Ceramic Powder Science*, (eds. G. L. Messing, E. R. Fuller Jr., H. Hausner), American Ceramic Society, Westerville, OH, 1988.

59. C. A. Finch, Applications of polyvinyl alcohol as a binder, pp. 539-648 in *Polyvinyl Alcohol-Developments* (Ed. C. A. Finch), Wiley, Chichester, U.K., 1992.

60. J. S. Reed, *Introduction to the Principles of Ceramic Processing*, Wiley, New York, 1988.

61. F.M. Tiller and C-D. Tsai, Theory of Filtration of Ceramics: I, Slip Casting, Journal of the American Ceramic Society 69 (1986) 882-887.

62. I. Tsao and R. Haber, The Characterization of Cake Structure and Rheology via Pressureless Slip Casting, Journal of Materials Science 28 (1993) 3214-3220.

63. A. G. Haerle and R. G. Haber, Experimental Evaluation of a New Flocculation-Filtration Model for Ceramic Shape Forming Process, Journal of the American Ceramic Society 79 (1996) 2385-96.

64. C-Y. Lin and B. J. Kellett, General Observations of Constant Flow Rate Filter Pressing, Journal of the American Ceramic Society 81 (1998) 2093-108.

65. T. Banno, S. Sano and K. Oda, Two-Dimensional Simulation of Cake Growth in Slip Casting, Journal of the American Ceramic Society 81 (1998) 2933-41.

66. Y. Gu and G. Meng, A Model for Ceramic membrane Formation by Dip-Coating, Journal of the European Ceramic Society 19 (1999) 1961-1966.

67. G. W. Scherer, Theory of Drying, Journal of the American Ceramic Society 73 (1990) 3-14.

68. J.E. Burke, Recrystallization and Sintering in Ceramics, pp. 17-38 in *Sintering Key Papers* (eds S. Somiya and Y Moriyoshi), Elsevier Applied Science, London and New York, 1990.

69. H. E. Exner, Solid State Sintering: Critical Assessment of Theoretical Concepts and Experimental Methods, pp. 87-100 in *Sintering Key Papers* (eds S. Somiya and Y Moriyoshi), Elsevier Applied Science, London and New York, 1990.

70. H. E. Exner and E. Arzt, Sintering Processes, pp. 157-184 in *Sintering Key Papers* (eds S. Somiya and Y Moriyoshi), Elsevier Applied Science, London and New York, 1990.

71. G. C. Kuczynski, Model Experiment and the Theory of Sintering, pp. 501-508 in *Sintering Key Papers* (eds S. Somiya and Y Moriyoshi), Elsevier Applied Science, London and New York, 1990.

72. G. Petzow and H. E. Exner, Particle Rearrangement in Solid State Sintering, pp. 639-655 in *Sintering Key Papers* (eds S. Somiya and Y Moriyoshi), Elsevier Applied Science, London and New York, 1990.

73. F. Parhami and R. M. McMeeking, A Network model for Initial Stage Sintering, Mechanics of Materials, 27 (1998) 111-124.

74. E. A. Olevsky, Theory of Sintering: from Discrete to Continuum, Materials Science and Engineering R23 (1998) 41-100.

75. R. M. German, Fundamentals of Sintering, pp.260-269 in Engineering Materials Handbook, Vol. 4 (ed. S. Schneider) ASM International USA, 1991.

76. R. K. Bordia and R. Raj, Sintering Behaviour of Ceramic Films Constrained by a Rigid Substrate, Journal of the American Ceramic Society 68 (1985) 287-292.

77. T. J. Garino and H.K. Bowen, Deposition and Sintering of Particle Films on a Rigid Substrate, Journal of the American Ceramic Society 70 (1987) C315-C317.

78. T. J. Garino and H. K. Bowen, Kinetics of Constrained-Film Sintering, Journal of the American Ceramic Society 73 (1990) 251-257.

79. D. R. Carroll and M. N. Rahaman, An Initial Stage Model for the Sintering of Constrained Polycrystalline Thin Films, Journal of the European Ceramic Society 14 (1994) 473-479.

80. W. Zhang and J. H. Schneibel, Calculations of Internal Stresses During Sintering in Two Dimensions. Journal of the American Ceramic Society 79 (1996) 2141-2144.

81. G. W. Scherer and T. J. Garino, Viscous Sintering on a Rigid Substrate. Journal of the American Ceramic Society 68 (1985) 216-220.

82. T. Cheng and R. Raj, Flaw Generation During Constrained Sintering of Metal-Ceramic and Metal-Glass Multilayer Films, Journal of American Ceramic Society, 72 (1989) 1649-55.

83. K-N. P. Kumar, K. Keizer, A.J. Burggraaf, T. Okubo and H. Nagamoto, Textural Evolution and Phase Transformation in Titania Membranes: Part 2 - Supported Membranes, J. Mater. Chem. 3 (1993) 1151-1159.

84. X. Yang and M. N. Rahaman, Thin Films by Consolidation and Sintering of Nanocrystalline Powders. Journal of the American Ceramic Society 71 (1997) 525-535.

85. S. Mayadevi, S. S. Kulkarni, A. J. Patil, M. H. Shinde, H. S. Potdar, S. B. Deshpande and S. K. Date, Controlled Chemical Precipitation of Titania for Membrane Applications – Effect of Heat Treatment and Fabrication Conditions on Its Performance, Journal of Material Science 35 (2000) 3943-3949.

86. M. Stech, P. Reynders and J. Rödel, Constrained Film Sintering of Nanocrystalline TiO_2, Journal of the American Ceramic Society 83 (2000) 1889-1896.

87. J. T. M. De Hosson, J. Hooijmans and R. Popma, Sintering Behaviour of Nanoceramic Coatings. Surface Engineering 16 (2000) 245-249.

88. P. Wang, P Huang, N. Xu, J. Shi and Y.S. Lin, Effects of Sintering on Properties of Alumina Microfiltration Membranes, Journal of Membrane Science 155 (1999) 309-314.

89. A. Akash and M. J. Mayo, Pore Growth during Initial-Stage Sintering, Journal of the American Ceramic Society 82 (1999) 2948-52.

90. ASTM C 693-74 (Reapproved 1980), “Standard Test Method for Density of Glass by Buoyancy”, 3 p.

91. ASTM C 373-88, “Standard Test Method for Water Absorption, Bulk Density, Apparent Porosity, and Apparent Specific Gravity of Fired Whiteware Products”, 2 p.

92. EN 623-2, “Methods of testing advanced technical ceramics – General and textural properties – Part 2: Determination of density and porosity”, 14 p.

93. S. Lowell and J. Shields, *Powder Surface Area and Porosity*, Powder Technology Series, Chapman & Hall, London, UK, 1984, 234 p.

94. ASTM F316-85, “Standard Test Methods for Pore Size Characteristics of Membrane Filters by Bubble Point and Mean Flow Pore Test”, 6 p.

95. C. Gelinas and R. Angers, Improvement of the Dynamic Water-Expulsion Method of Pore Size Distribution Measurements, American Ceramic Society Bulletin 65 (1986) 1297-1300.

96. N. Laitinen, Development of a Ceramic Membrane Filtration Equipment and Its Applicability for Different Wastewaters, PhD Thesis, Lappeenranta University of Technology, 2002, 126 p.

97. N. Laitinen, D. Michaud, C. Piquet, N. Teilleria, A. Luonsi, E. Levänen and M. Nyström, Effect of Filtration Conditions and Backflushing on Ceramic Membrane Ultrafiltration of Board Industry Wastewaters, Separation and Purification Technology 24 (2001) 319-328.

98. N. Laitinen, A. Luonsi, E. Levänen and M. Nyström, Effect of Backflushing Conditions on Ultrafiltration of Board Industry Wastewaters with Ceramic Membranes, Separation and Purification Technology 25 (2001) 323-331.

99. A. Luonsi, N. Laitinen, K. Beyer, E. Levänen, Y. Poussade and M. Nyström, Separation of CTMP Mill-Activated Sludge with Ceramic membranes, Desalination 146 (2001) 399-404.

100. N. Laitinen, M. Kulovaara, E. Levänen, A. Luonsi, N. Teilleris and M. Nyström, Ultrafiltration of Stone Cutting Mine Wastewater with Ceramic Membranes – a Case Study, Desalination 149 (2002) 121-125.

101. N. Laitinen, E. Levänen, A. Luonsi, T. Mäntylä and J. Vilen, Ceramic Membrane Filtration for Recycling Wastewater, Regional Environmental Publications 74, Pirkanmaa Regional Environment Centre, Tampere 1998 (in Finnish).

102. M. Kolari, Preparation and Characterization of Alumina UltrafiltrationUltra filtration Membranes. Tampere University of Technology. Lic.Tech. Thesis (1997) 93 p. (in Finnish)

103. J. B. Rosenholm, T. Mäntylä and A. Yli-Urpo, Synthesis and Properties of High Performance Ceramic Oxides with Focus on Porous Structures: Membranes, Filters and Biomaterials, pp. 91-115 in *National Programme on Materials and Structure Research* (ed. J. Pirttijärvi) Publications of the Academy of Finland 2/96, Edita, Helsinki, 1996.

104. J. B. Rosenholm, T. Mäntylä and A. Yli-Urpo, Synthesis and Properties of High Performance Ceramic Oxides with Focus on Porous Structures: Membranes, Filters and Biomaterials (eds. M. Linden, E. Levänen and M. Jokinen), Turku, 2000, 96 p.

105. T. Koiranen, Corrosion of Porous Ceramics, Tampere University of Technology, Institute of Materials Science, M.Sc Thesis (1995) 92 p. (in Finnish)

Publication I

P. Mikkola, P. Ylhä, E. Levänen and J.B. Rosenholm

Effect of Impurities on Dispersion Properties of alpha-alumina Powder

Ceramics International, 30 (2004)

Publication II

E. Levänen, T. Mäntylä, P. Mikkola, J. B. Rosenholm

Influence of Additives on Capillary Absorption of Aqueous Solutions into Symmetric Porous Ceramic Substrate

Journal of Colloid and Interface Science, 234 (2001)

Publication III

E. Levänen, T. Mäntylä, P. Mikkola and J. B. Rosenholm

Layer Buildup onto Two-layered Porous Substrate by Dip-Coating: Modeling and Effect of Additives on Growth Rate

Journal of Colloid and Interface Science, 230 (2000)

Publication IV

P. Mikkola, E. Levänen, T. Mäntylä and J.B. Rosenholm
Colloidal Processing of Aluminum Oxide Powder for Membrane Applications
Ceramics International, 29 (2003)

Publication V

E. Levänen and T. Mäntylä

Effect of Sintering Temperature on Functional Properties and Microstructure of Free-Standing and Supported alumina Membranes

Journal of the European Ceramic Society, 22 (2002)

Publication VI

N. Laitinen, A. Luonsi, E. Levänen, L. Grönroos, T. Mäntylä and M. Nyström

Modified and unmodified alumina membranes in ultrafiltration of board mill wastewater fractions

Desalination, 115 (1998)

Tampereen teknillinen yliopisto
PL 527
33101 Tampere

Tampere University of Technology
P.O. Box 527
FIN-33101 Tampere, Finland